TWO-DIMENSIONAL SUBSONIC WIND TUNNEL TESTS OF TWO 15-PERCENT THICK CIRCULATION CONTROL AIRFOILS

by

Robert J. Englar

Technical Note AL-211

August 1971

NAVAL SHIP RESEARCH AND DEVELOPMENT CENTER
BETHESDA MARYLAND 20034

TWO-DIMENSIONAL SUBSONIC WIND TUNNEL TESTS OF TWO 15-PERCENT THICK CIRCULATION CONTROL AIRFOILS

by

Robert J. Englar

Work performed under sponsorship of the Office of Naval Research, Aeronautics, Code 461, under Project Order #1-0140, NR 212-204

August 1971

Technical Note AL-211

TABLE OF CONTENTS

LIST OF FIGURES

LIST OF FIGURES (Cont.)

LIST OF FIGURES (Cont.)

SYMBOLS

a_j	Sonic velocity in the jet, ft/sec
c	Chord length, ft
C_d	Sectional profile drag coefficient from momentum loss in wake, corrected for additional mass efflux of the jet
C_{d_e}	Equivalent drag coefficient, $C_d + C_\mu \frac{V_j}{2V_\infty} + C_\mu \frac{V_\infty}{V_j}$
C_ℓ	Sectional lift coefficient
$C_{\ell_{max}}$	Maximum sectional lift coefficient obtainable within test C_μ limitations
$C_{m_{50}}$	Pitching moment coefficient about the half-chord
C_p	Pressure coefficient, $\frac{P_\ell - P_\infty}{q_\infty}$
C_μ	Momentum coefficient, $\dot{m}V_j / (q_\infty S)$
d	Profile drag corrected for jet mass efflux, lbs
d_e	Equivalent drag, lbs, $d + \frac{\dot{m}V_j^2}{2V_\infty} + \dot{m}V_\infty$
h	Slot height, in
ℓ	Sectional lift, lb
ℓ/d_e	Equivalent section lift-drag ratio
$\dot{m}$	Mass efflux, slugs/sec
M_j	Mach number in the jet
M_∞	Free stream Mach number
P_ℓ	Local static pressure on the model, lb/ft^2
P_t	Duct (plenum) total pressure, lb/ft^2
P_∞	Free stream static pressure, lb/ft^2
q_∞	Free stream dynamic pressure, lb/ft^2
R	Universal gas constant, 1715 $ft^2/sec^2\ {}^\circ R$
R_e	Reynolds number based on chord
S	Model planform area, ft^2

SYMBOLS (Cont.)

T_j	Jet static temperature, $^{\circ}R$
T_t	Duct (Plenum) total temperatrue, $^{\circ}R$
V_j	Jet velocity, ft/sec
V_∞	Free stream velocity, ft/sec
x	Chordwise distance from leading edge, ft
x/c	Dimensionless chordwise position
α	Geometric angle of attack, deg
γ	Ratio of specific heats

SUMMARY

Two relatively thin Circulation Control (CC) elliptic airfoils were tested subsonically to determine their characteristics as proposed helicopter rotor tip sections. These airfoils, employing tangential trailing edge (Coanda) blowing, had shown very promising transonic characteristics in previous tests. It was the purpose of the subsonic retests to determine if these thin sections could generate low speed characteristics which would be equally impressive. Due to its more forward slot location, the 15-percent thick pure elliptic section displayed effective subsonic operation at positive angle of attack, reducing drag while producing lift coefficients up to 3.5. The rounded trailing edge configuration, with further aft slot and better Coanda deflection of the jet, generated lift coefficients up to 4.25 (with a preference for negative incidence), but experienced higher drag levels. As a result of the small nose radii and low test Reynolds number, both sections were limited in performance by leading edge separation. At a fixed momentum coefficient, variation in slot height indicated that better performance was obtained for reduced heights. This was due primarily to higher energy levels in the jet sheet, but the lower bound on slot height was limited by boundary layer buildup in very small nozzles. Comparison of both CC sections to the more conventional NACA 0012 blade section indicated far greater lift capabilities with circulation control. However, due to blowing power requirements, equivalent efficiency was less at positive incidence than for the conventional section.

INTRODUCTION

Previous transonic tests (Reference 1) of relatively thin Circulation Control (CC) airfoils had revealed very promising characteristics for application to helicopter rotor tip sections. This effective performance of the CC airfoils, which employed tangential trailing edge blowing, was obtained if detachment of the Coanda jet could be delayed or prevented. One of the models tested, a pure elliptic CC section of 15-percent thickness-to-chord ratio, was able to control the jet detachment, and thus showed effective high speed performance based on its ability to:

1. Maintain good transonic equivalent lift-drag ratios at relatively high lift coefficient,
2. Reduce drag by thrust recovery in a manner similar to jet flap devices and thus increase the drag divergent Mach number,
3. Control shock wave location and associated boundary layer separation.

However, an effective rotor tip section must also satisfy the cyclic requirements of the rotor to alternately operate in the subsonic flow regime experienced by the retreating blade.

It has been shown (e.g., References 2, 3, 4, 5) that modified elliptic CC sections, employing variations in thickness, slot height, trailing edge radius, and camber, have been able to generate very high lift coefficient and equivalent lift-drag ratios, both at subsonic speeds and small angles of attack. It was the purpose of the present tests to determine if the two thin transonic CC elliptic sections would also be able to generate these impressive subsonic characteristics. Also desired were their aerodynamic characteristics over a wide angle of attack range ($-20^{\circ} \leq \alpha \leq +20^{\circ}$), which would allow comparison to a more conventional rotor section such as the NACA 0012. Determination of the influence of variation in slot height and location was an additional objective.

MODELS AND TEST APPARATUS

Of the three model sections tested transonically (Reference 1), the two tangentially blown ellipses were chosen for the subsonic retests. The two differ only in the geometries of their trailing edges, which are interchangeable in a common leading edge. Details of their design criteria and constructions are presented in Reference 1 and are thus omitted here. Their geometries as retested are shown in Figure 1 of this report. The major characteristics of each model are discussed below, along with any minor changes necessary for subsonic tests.

MODELS

The basic model was an uncambered geometric ellipse of 15-percent thickness-to-chord ratio, hereafter referred to as the "pure ellipse". An 8-inch chord and an upper surface tangential slot at 7.39 inches from the leading edge yielded a slot position of 92.4 percent chord. The 0.09-inch trailing edge radius of the pure ellipse produced a radius-to-chord ratio of 0.01225. This basic trailing edge was interchangeable with another having a larger radius of 0.31 inch, which reduced the overall chord to 7.70 inches. This second model, referred to as the "rounded ellipse" thus had a thickness-to-chord ratio of 15.6 percent, a trailing edge radius-to-chord ratio of 0.0403, and a slot location of 96 percent. Both models were constructed of 0.25-inch fiberglass finished to 600 fineness. A steel blade formed the upper surface of the slot and was so situated that the slot exit was the minimum area throat of a smoothly converging nozzle. Two modifications to the models were made: the addition of separate high pressure internal plenums at each end of the span, and flow fences, both of which are discussed below.

TEST APPARATUS AND TECHNIQUE

The two-dimensional tests were conducted in the NSRDC 15" x 20" subsonic tunnel which has a 16:1 contraction ratio and a partially open test section. Plexiglass tunnel walls allowed flow visualization by means of both tufts and oil flow, the latter making use of an ultra-violet light and fluorescent die. Both models were pressure tapped along the center span as denoted in Figure 1. Lift and pitching moment

coefficients were obtained by numerical integration of pressures from those taps as recorded on a 144 port multiple scannivalve readout. These coefficients were corrected by adding the vertical jet reaction component to lift, and both horizontal and vertical jet components to the pitching moment. Standard solid blockage corrections were applied to free stream dynamic pressure; no wake blockage corrections were used due to uncertain effect of the jet. Comparison of test pressure distribution near the mid-chord agreed very well with potential flow, thus indicating that streamline curvature (camber) effects were negligible. In addition, experimental pressure distributions (see for example Figure 23) very clearly showed that $C_p = 1.0$ was being calculated from measurements at the leading edge stagnation point, thus indicating that corrected values of q_∞ were very close to the true values.

Drag measurements were made using a wake rake approximately 1.5 chord lengths downstream of the model. This rake employed 54 total pressure and 8 static pressure tubes in a 15-inch height, with the tubes more heavily concentrated near the centerline. The momentum deficit methods of both Jones and Betz (Reference 6) were used to reduce the pressure data to coefficient form. To account for additional momentum from the jet, it was necessary to correct the drag coefficient of both methods by the addition of $\dot{m}V_\infty/q_\infty S$, as noted in Reference 5. The rake itself was inclined upwards 10 degrees from the free stream to compensate for any angularity errors due to the turning influence of the jet.

To assure that test conditions were in actuality as close to two-dimensional as possible, especially in the high lift cases, several additional techniques were employed. Because very high trailing edge suction peaks and associated adverse pressure gradients were characteristic of these sections, strong trailing edge vorticity frequently formed as the adverse gradients and tunnel wall boundary layers interacted. To counteract this, separate internal plenums were installed in the model at each end with regulated high supply pressure separate from the main plenum. (See Reference 2 for details.) When properly adjusted for each test condition (i.e., blowing coefficient and angle of attack),

these "tip jets" were able to energize the wall boundary layer and greatly reduce or even eliminate the trailing vortices and associated induced effects. However, the increased velocity and mass efflux from the tip jets tended to exit three-dimensionally, interfering with the lesser velocity main plenum flow and producing some spanwise variation. To prevent this, thin flow fences were installed between the tip jets and main plenum. These confined the tip jets to a narrow channel near the tunnel wall, where they could still strongly affect the vorticity. The resulting two-dimensionality was then verified by spanwise static taps located near the trailing edge, and the required tip jet pressure was ascertained by a cotton tuft which would cease to spin when the vorticity was eliminated.

Mass flow rate ($\dot{m}$) was measured by an orifice plate inserted in the main supply line and calibrated for Reynolds number effects. Jet velocity (V_j) was calculated assuming an isentropic expansion from duct (plenum) total pressure to free stream static pressure:

$$V_j = a_j M_j = \sqrt{\gamma R T_j}\, M_j = \left\{ 2RT_t \left(\frac{\gamma}{\gamma-1} \right) \left[1 - \left(\frac{p_\infty}{p_t} \right)^{\frac{\gamma-1}{\gamma}} \right] \right\}^{\frac{1}{2}}$$

The momentum coefficient was then defined as

$$C_\mu = \frac{\dot{m} V_j}{q_\infty S}$$

A static calibration of nozzle height expansion under pressure allowed a determination of the isentropic mass flow rate, and thus the ratio of measured to isentropic $\dot{m}$ could be determined. This ratio was found to be between 0.90 and 0.96 over the entire duct pressure range, thus indicating the relative efficiency of the nozzle.

DESIGN AND TEST CONSIDERATIONS

The basic design considerations for the present models were those relating primarily to effective transonic performance (Reference 1), with no new design changes being made for the subsonic tests. It should be noted that, whereas the pure elliptic shape was the superior of the two transonically (where the jet detachment criteria was of such importance), it would be expected that subsonically the rounded ellipse should be the better performer due to its very effective Coanda jet turning and resultant high lift augmentation. (See Reference 7 for more detailed discussion of subsonic CC design.) It is necessary to place some reservation on this prediction, because angle of attack and slot location can strongly influence the subsonic effectiveness of CC sections. Figure 2 presents potential flow pressure distributions for the pure ellipse at $C_\ell \approx 1.0$. Usual design procedure is to locate the slot slightly ahead of the adverse pressure gradient, which, except for higher positive angles of attack, is far aft on the airfoil. This location leads to high energy levels in the Coanda jet and assures favorable jet attachment and turning, and thus high lift augmentation at small or negative incidences. However, at positive angles of attack, the adverse pressure gradient is farther upstream, and the far aft slot has a reduced effect on it. Reference 3 indicates that for constant blowing (C_μ = constant) at positive incidence, forward movement of the slot produces an appreciable increase in stalling angle of attack while maintaining a constant lift curve slope. This result is due primarily to a re-energizing of the upstream boundary layer and prevention of upper surface separation. It is, unfortunately, also associated with reduced $C_{\ell_{max}}$ since the energy level in the jet has been reduced when it reaches and attempts to negotiate the trailing edge curvature. Thus an important aspect of the present tests was to observe any increase in performance at positive incidence produced by the pure ellipse, with a slot location about 3.6 percent chord ahead of the rounded configuration.

Although Reynolds number effects on scaling should be very small (since a full scale blade should only have two to three times the chord

of the model), a series of preliminary runs was made at variable free stream dynamic pressure (from 5 to 55 psf) and thus variable R_e. At low blowing, curves of C_ℓ vs. C_μ for q_∞ = 55 psf showed only a slight deviation from those at q_∞ = 20 psf. As C_μ was increased the curves tended to coincide, thus indicating an entrainment of flow into the boundary layer, and apparent elimination of variation with Reynolds number. From a practical standpoint, it was desirable to run at a lower q_∞, since a given duct pressure range would then yield a larger range of C_μ. Thus, the data published herein is all for a free stream dynamic pressure of 20 psf and Reynolds numbers in the range of 520,000 to 550,000. The upper limit of C_μ was determined from the duct pressure at which the jet sheet impinged on the tunnel floor, yielding separation of the floor boundary layer and causing "wash out" of the rake and diffuser. In certain cases of very high trailing edge suction peaks, pressure coefficients as high as -18.0 were generated, thus reaching the limits of the 2.5 psid transducers in the scannivalve. Based on these two limitationsand depending on slot height, duct pressure maxima of 50 and 40 in. Hg. were set for the pure and rounded ellipse, respectively. Figure 3 presents the measured momentum coefficients associated with the range of duct pressures for several slot heights on both models, while Figure 4 presents the corresponding ratios of isentropic jet velocity to measured free stream velocity. The much higher range of C_μ for the pure ellipse was available because the smaller trailing edge radius did not allow large jet turning angles before detachment, and thus the restrictions of floor impingement and high negative pressures were avoided. It should be noted that, due to the high mass flow rates and/or plenum pressures required, very large values of momentum coefficient are not of practical usage for application to CC rotors. A reasonable and practical upper limit might be on the order of $C_\mu \leq 0.30$.

RESULTS AND DISCUSSION

PURE ELLIPTICAL TRAILING EDGE

Lift

The 15-percent pure elliptic section was subjected to testing over the angle of attack range $-12^{\circ} \leq \alpha \leq 20^{\circ}$, with momentum coefficients $0 \leq C_{\mu} \leq 0.77$ and for two slot heights, h = 0.01 inch and 0.025 inch. Figures 5 and 6 present lift data as a function of C_{μ} for constant α and slot height. The initial sharp rise in the curves at low blowing is usually attributed to boundary layer control, and the reduced slope at higher C_{μ} is a result of supercirculation. Note that there did not appear to be any lift drop-off with increased blowing ("C_{μ} stall") at any angle of attack, and that the maximum lift augmentations of 30 (Figure 7) occurred at the very low values of blowing. A maximum lift coefficient of less than 2.8 for $C_{\mu} \leq 0.30$ does not appear outstanding in the light of other CC results, (e.g., References 4, 5, 8, and 10) and the lack of extreme high lift capability can be attributed to several conditions: (1) absence of large trailing edge radius associated with strong Coanda flow turning; (2) more forward slot location than usual (i.e., 95-96 percent chord), leading to a lower energy level in the jet at the trailing edge, and (3) sharp nose radius producing leading edge separation. With regard to this last point, a thorough analysis of pressure distributions in the nose region (especially in the peaky cases of high α or increased C_{ℓ}) indicated that the bends in the lift curves of Figures 5 and 6 were very closely associated with the pressure rise (suction peak drop) characteristic of a local separation. The fact that this phenomenon was very localized and was not accompanied by complete upper surface separation points strongly to the leading edge laminar separation bubble. Figure 8 depicts details of the formation of this bubble at α = 3 degrees, h = 0.01 inch. It should also be stated that this problem could quite likely be influenced by the low test Reynolds number, which suggests that the high lift conditions should be rerun at increased q_{∞}.

A direct comparison of lift characteristics of Figures 5 and 6 by plotting on the same C_μ scale reveals the effect of slot height variation. In the range of $C_\mu \leq 0.30$, the 0.025-inch slot height produced a C_ℓ reduction of as much as 13 percent of the corresponding (same C_μ and α) value for h = 0.01 inch. The reason for the reduced performance of the larger slot height is complex and not fully understood, but is probably dependent on jet Reynolds number and on mixing characteristics of the enlarged jet with the associated boundary layer. It is rather apparent, however, that for the same C_μ, the larger slot height required a much lower plenum pressure, producing a reduced jet velocity, (Figures 3 and 4). The kinetic energy flux in the jet, a function of V_j^3, was thus reduced accordingly; these lower jet energy levels at the Coanda surface were probably directly related to the degradation of performance.

Whereas the 92.4 percent slot location was not particularly effective in yielding high lift, Figure 9 (in comparison with Figure 26) shows that it was in fact quite able to extend the range of positive α operation. Unlike the far aft locations, this slot position yielded an increase in C_ℓ for an increase in positive incidence at constant C_μ. However, with increasing C_μ, the "α-stall" occurred at progressively lower angles of attack.

An interesting feature of tangential blowing over bluff trailing edges was its apparent ability to exhibit viscous flow section properties very close to those predicted inviscidly by potential flow. Figure 10 shows comparison between test and theoretical data for both blown and unblown cases, where the discrepancy for the unblown case was primarily in the separated regime at the trailing edge. Application of blowing caused very close agreement over the entire airfoil except: (1) downstream of the slot where the additional suction peak was produced by the jet velocity (not predictable by potential flow alone) and (2) in the lower surface trailing edge separation bubble region. Evaluation of the wall jet contribution to the area under the C_p curve allowed calculation of the potential flow results for a reduced net C_ℓ which excluded this additional area. The agreement between test and theory was then even better.

An additional capability of circulation control sections is shown in Figure 11, that being the generation of positive lift at negative angles of attack. For no blowing, it is seen that the section behaved as a conventional airfoil at negative incidence, generating a negative lift due predominantly to lower surface suction. As blowing was applied and increased, that condition was reversed. Suction was transferred to the upper surface, with the lower surface contributing very little to lift except at the trailing edge. The net result was a positive C_ℓ at negative α due primarily to supercirculation around the airfoil. This represents a capability clearly not available from a conventional section, and relative to the negative inflow angles frequently encountered in rotary wing application, marks a quite desirable trait. Also noticeable in Figure 11 for the $C_\mu = 0.202$ case is a local pressure rise at the second pressure tap downstream from the slot. This occurred quite frequently at the higher blowing rates for both negative and positive incidence. Since its location was in the region of rapid curvature change in the vicinity of the slot exit, this behavior was attributed to a small separation bubble formed by the high velocity jet unable to negotiate the sharp radius variation. As reattachment occurred immediately downstream, the overall effect appeared to be negligible other than a very slight loss in C_ℓ.

Drag

The effect of thrust recovery on section drag coefficient is indicated in Figures 12 and 13, where for $\alpha \leq +6^\circ$ the pure ellipse performed very much as a jet flap. This was a result of the small trailing edge radius, which was not conducive to effective jet sheet turning. Consequently, the jet detached from the Coanda surface at a location closer to the slot and at a smaller angle relative to the free-stream. This resulted in higher wake energy levels, lower mixing losses and thus larger drag reductions over the unblown cases. Other factors contributing a less important but noticeable drag reduction were high leading edge suction peaks (before laminar bubble formation) and an increase in lower surface base pressure with blowing. Above 6 degrees

angle of attack, the drag no longer decreased with C_μ; in most cases it increased. Reference to Figure 5 indicates that this rise in drag occurred in the same regions at which the lift degradation began. Study of the corresponding pressure distributions confirmed that the drag increase began at that value of C_μ where the nose separation bubble formed, followed in many cases at higher α by separation over larger areas of the upper surface.

Pitching Moment

Typical of tangentially blown sections is the suction peak at the trailing edge and resulting nose-down pitching moment. Figures 14 and 15 depict the half-chord (probable location of a CC helicopter blade spar) pitching moment for the pure ellipse, which because of its elongated trailing edge, did not exhibit such large suction peaks as the more rounded configuration. The moment coefficient did become more negative with increased C_μ, but nowhere near as rapidly as the rounded trailing edge (e.g., Figure 18 of Reference 1). However, at higher α when the nose suction peak was reduced, the trailing edge peak became more dominant and the $C_{m_{50}}$ more negative.

Equivalent Lift-Drag Ratio

Section performance can best be determined in terms of an equivalent lift-drag ratio (ℓ/d_e) which takes into account a penalty for the kinetic energy required for blowing, and thus allows direct comparison to unblown airfoils. The equivalent drag is defined as (see pages 8 and 9; Reference 1):

$$d_e = d + \frac{\dot{m}V_j^2}{2V_\infty} + \dot{m}V_\infty$$

where d is the momentum deficit drag in the wake (corrected for jet mass efflux), the second term is the kinetic energy flux and the third term is a ram or intake penalty. In coefficient form, the equivalent lift-drag ratio may then be written as:

$$\ell/d_e = C_\ell \Big/ \left[C_d + C_\mu \frac{V_j}{2V_\infty} + C_\mu \frac{V_\infty}{V_j} \right]$$

Figures 16 and 17 depict this parameter as a function of lift coefficient for constant angle of attack (where the few points at negative C_ℓ and ℓ/d_e have been omitted as of little interest). The maximum efficiencies at negative and zero incidence occurred at low C_μ and C_ℓ, where at positive α the maxima occurred for the unblown cases [overall $(\ell/d_e)_{max}$ = 43.5 at $\alpha = 9^\circ$]. The forward slot location, small trailing edge radius, and nose separation bubble have combined to produce a configuration that obtained higher C_ℓ accompanied by some relative loss in efficiency. Nevertheless its ability to operate at positive angle of attack (Figure 18 plots $(\ell/d_e)_{max}$ over the α range) and lift coefficients up to 3.5 still make it a desirable rotor tip section in a regime where required C_ℓ is not extremely high and resultant inflow angles may frequently be positive.

ROUNDED TRAILING EDGE ELLIPSE

Lift

The rounded trailing edge configuration was tested subsonically over the angle of attack range $-20^\circ \leq \alpha \leq 9^\circ$, with momentum coefficients $0 \leq C_\mu \leq 0.33$, and for four slot heights: 0.010 inch, 0.025 inch, 0.050 inch and 0.005 inch. The momentum coefficient range was more limited than the pure ellipse due to the effective Coanda jet turning, with resulting very high negative pressure coefficients and impingement of the jet on the tunnel floor. Based on results from References 1, 5, 8, 9 and 10, the preference of the rounded trailing edge to operate at negative angles was anticipated, and angle of attack test range was shifted towards that regime. Figures 19 through 22 present the lift characteristics as a function of C_μ for the four slot heights. With the exception of h = 0.05 inch, the C_ℓ vs. C_μ curves were very steep and almost linear, indicating effective boundary layer control and high lift augmentation. However, at zero and positive incidence, the initially steep curves were subjected to large slope changes before very high C_ℓ was obtained. As was the case with the pure ellipse, this performance degradation was clearly attributable to the relatively

sharp leading edge and associated reduction in suction peak under high circulation. Here again, low Reynolds number may have contributed a significant effect. Figure 23 compares experimental pressure distributions for α = 3 degrees and h = 0.01 inch; the highest nose suction peak occurred for C_ℓ = 2.72, the point in Figure 19 where the slope change began. An increase in C_μ produced a drop in nose suction and a decrease in slope of the curve. However, as can be seen in Figure 23, the overall lift coefficient continued to increase as the nose loss was compensated for by increased suction over the mid chord. An important difference in this nose regime was noticed relative to the pure ellipse, which showed a very distinct separation bubble in the leading edge pressure distribution (Figure 8). The rounded configuration never displayed this characteristic as such, but as Figure 23 verifies, the nose peak gradually reduced with blowing until it reached a certain value of C_p (approximately -4.9 in this case but varying with α).

Comparison of lift coefficients at the same C_μ and α but different slot heights showed the same trends as for the pure ellipse: increase in slot height yielded reduced C_ℓ. The apparent cause was again lower energy levels in the jet with increased slot height. An exception was found for the very small (h = 0.005 inch) slot height, which showed inferior performance relative to the larger h = 0.01 inch slot. It is felt that the cause was a result of boundary layer buildup in the nozzle throat causing reduced Coanda effectiveness, as well as a result of difficulty in uniformly setting that small slot height on the model. Lift augmentations for two slot heights are presented in Figures 24 and 25, with the h = 0.01 inch height yielding almost twice the augmentation of the 0.025 inch slot. Figure 26 shows the effect of far aft slot position in generating high lift at negative incidence. An increase in blowing shifted $C_{\ell_{max}}$ towards a more negative angle of attack. However, except for the lower values of blowing, an increase in positive incidence (for constant C_μ) soon resulted in a decrease in lift, undoubtedly a disadvantage if operation at positive blade inflow angles were anticipated.

A comment should be made concerning the nonlinearity of the curves in Figure 21 for the 0.05 inch slot height at lower C_μ. Apparently, the increase in slot height sufficiently changed the external surface shape enough to effect the boundary layer transition on the upper surface. Oil flow studies and very closely spaced data points relating to a similar phenomenon in Reference 10 indicate that the reflex in the C_ℓ vs. C_μ curves actually approached a discontinuity in the curve immediately preceeding the change to a reduced slope.

Drag

Variation in drag coefficient with blowing is presented in Figures 27, 28 and 29 (Drag data and resulting ℓ/d_e for h = 0.005 inch are uncertain due to nozzle boundary layer and nonuniformity of the slot, and are thus not included). At negative α, and for low blowing rates at positive α, the rounded ellipse also performed as a jet flap with the excess momentum in the jet sheet after detachment producing a thrust resulting in zero or negative drag. However, for higher C_μ at positive α, the jet turning angle was greater. Delayed jet detachment (i.e., at a greater arc length downstream from the slot) caused mixing losses with the freestream and yielded the resultant low energy wake accompanied by a much enlarged wake width. Comparison of lift and drag curves (for example, Figures 19 and 27) indicated that the change in the lift slope corresponds exactly(same C_μ) to the sudden rise in drag, which implies that the drop in nose suction must have had some effect on the increase in drag. (The same result appeared true for the pure ellipse, although the drag increase was not so sudden.)

Pitching Moment

Pitching moment coefficients are presented in Figures 30 and 31 for two slot heights (the other two showed very similar trends). The high trailing edge suction peaks produced much greater nose-down moments than for the pure ellipse. At positive incidence, the rises in the curves were due to redistribution of lift over the forward portion of the upper surface (see Figure 23).

Equivalent Lift-Drag Ratio

Section efficiencies are presented in Figures 32, 33 and 34, where in spite of the high sectional lift coefficient, the rounded configuration generated equivalent lift-drag ratios of 40 or less at $C_\ell \approx 1.25$ and h = 0.01 inch. An unexpected result was that the maximum efficiencies occurred at positive incidence (Figure 35). It appears that the higher ℓ/d_e values were generated at low or zero blowing, thus indicating that the lift due to incidence dominated lift due to blowing in the regime of higher efficiency. A requirement to operate at higher lift obtained by blowing would thus be associated with an overall reduced efficiency. However, the need for high C_ℓ at the rotor tip section is doubtful, and if operation at $\alpha \leq 7^\circ$ is anticipated, a comparison of Figures 35 and 18 points to the rounded configuration as the more efficient. In both cases, it appears that an increase in slot height can be detrimental to efficiency.

COMPARISON

Variation in trailing edge radius on the two CC 15-percent thick sections, which were otherwise identical, yielded large differences in section properties. Figure 36 compares the maximum lifting characteristics, where it is seen that for the range of $C_\mu \leq 0.20$, the rounded trailing edge roughly doubles the values produced by the pure ellipse. The C_ℓ values shown for each α are maxima within the range of momentum coefficients $0 \leq C_\mu \leq 0.20$, the upper limit resulting from test limitations (floor impingement and transducer range) on the rounded ellipse with h = 0.01. Since this value was not the limit for the remaining configurations, these data are not be taken as section overall maximum C_ℓ. Data for a conventional rotor section, the NACA 0012 (from Reference 11) at $M_\infty = 0.2$ is plotted for comparison to the CC sections (at $M_\infty = 0.12$). Its lifting capability is restricted by the Kutta condition at the sharp trailing edge, a condition overcome by the bluff trailing edge of the CC sections and their ability to control circulation by movement of the stagnation point. Whereas the drag on the blown sections can be reduced to far less than that of the 0012,

the power required as reflected in the parameter ℓ/d_e reduced the CC efficiency to less than half that of the unblown 0012, as seen in Figure 37. (The comparison is being made for airfoils of unlike thickness, where the additional 3-3.6 percent was somewhat detrimental to CC profile drag, but due to somewhat larger nose radius, was helpful in lift. In addition, the 0012 was tested at $R_e = 12 \times 10^6$ which would introduce further differences between the two tests.) Clearly, the advantage of these thin circulation control sections does not lie in high efficiency, but rather in their ability to generate a large range of lift coefficients over a wide range of positive and negative angle of attack. Coupled with the pure ellipse's transonic performance, this ability to operate cyclically with performance variation from blowing, instead of change in incidence, should provide the basis for much improvement in rotor tip section design. Figure 38 presents a comparison of both subsonic ($M_\infty = 0.3$) and transonic ($M_\infty = 0.7$) performance, where all data on the solid curves for the pure ellipse are comparable to only the two points for the 0012 for the same small angle, $\alpha = 0.8$ degrees.

CONCLUSIONS

Subsonic tests conducted on two 15-percent thick circulation control ellipses indicated that subsonic performance was heavily dependent on prevention of leading edge separation at higher lift coefficient. Comparison of experimental data over a wide range of angle of attack and momentum coefficient yielded the following conclusions:

- The pure elliptic configuration, due to its more forward slot location, displayed increased upper surface boundary layer control, and was thus able to operate effectively at positive angles. Its small trailing edge radius prevented good Coanda turning, resulting in maximum lift coefficients of 2.8 and lift augmentation ratios of 30 for $C_\mu \leq 0.30$ but reduced nose-down pitching moment. The excess energy in the jet sheet after detachment greatly reduced drag, thus generating maximum equivalent efficiencies of 43 at $C_\ell \approx 1.0$.

- The larger trailing edge radius of the rounded ellipse generated strong Coanda attachment, resulting in preference for negative angles, where a maximum C_ℓ of 4.25 was generated at $\alpha = -6^\circ$ and $C_\mu \leq 0.30$, along with associated lift augmentations of 67. Drag levels were generally higher than those of the pure ellipse, resulting in a maximum ℓ/d_e of 40 at $C_\ell = 1.25$.

- Due to higher energy levels in the jet sheet, the 0.01 inch slot height for both models was more effective than larger values. The reduced performance of the 0.005 inch height on the rounded ellipse was probably due to boundary layer buildup in the nozzle throat and resulting poor Coanda flow.

- Comparison of the CC sections to the conventional NACA 0012 indicates much higher lift capabilities over a wider angle of attack range for the blown sections. However, due primarily to the penalty for blowing paid by the CC sections, the 0012 generated twice the efficiency at higher positive α.

These results indicate that a thin circulation control section capable of good transonic performance can also perform well in the subsonic regime over a wide angle of attack range. The present tests suggest that future investigations be conducted on larger leading edge radii (or perhaps ovoid shaped noses), variation in longitudinal slot location, and a composite trailing edge configuration based on the promising features of both the pure and rounded ellipses. In addition, testing at higher Reynolds number should be seriously considered.

Aviation and Surface Effects Department
Naval Ship Research and Development Center
Bethesda, Maryland 20034
August 1971

ACKNOWLEDGEMENT

The author would like to express his appreciation to Mr. M. Stone for his valuable assistance in the testing of the pure elliptic configuration in May - June 970, and Mr. P. Deal, who helped conduct the tests on the rounded trailing edge ellipse in May 1971.

REFERENCES

1. Englar, Robert J. Two-Dimensional Transonic Wind Tunnel Tests of Three 15 Percent Thick Circulation Control Airfoils, Washington, Dec. 1970. 70 l. incl. illus. (Naval Ship Research and Development Center. Tech. Note Al-182)

2. Williams, Robert M. Some Research on Rotor Circulation Control. In CAL/AVLABS Symposium: Aerodynamics of Rotary Wing and V/STOL Aircraft. 3rd, Buffalo, Jun 1969. Proceedings, Vol. 2.

3. Jones, Dale G. The Performance of Circulation Control Airfoils. Cambridge, Eng., Jul 1970. (Cambridge Univ. Ph.D. Thesis)

4. Kind, R. J. and D. J. Maull. An Experimental Investigation of a Low-Speed Circulation - Controlled Aerofoil. Aeronautical Quarterly, Vol. XIX, May 1968.

5. Williams, Robert M. and Harvey J. Howe. Two Dimensional Subsonic Wind Tunnel Tests on a 20 Percent Thick, 5 Percent Cambered Circulation Control Airfoil. Wash., Aug 1970. 23 l. incl. illus. (Naval Ship Research and Development Center. Tech. Note AL-176) (AD 877-764)

6. Schlichting, Hermann. Boundary Layer Theory. 6th ed., N. Y., McGraw-Hill, 1968.

7. Williams, Robert M. Design Considerations of Circulation Control Airfoils. (Naval Ship Research and Development Center. Tech. Note AL-185), (In preparation)

8. Englar, Robert J. Two-Dimensional Subsonic Wind Tunnel Tests on a Cambered 30-Percent Thick Circulation Control Airfoil. (Naval Ship Research and Development Center. Tech. Note AL-201),(In preparation)

9. Englar, Robert J. and Robert M. Williams. Design of a Circulation Control Stern Plane for Submerine Applications. (Naval Ship Research and Development Center. Tech. Note AL-200), (In preparation)

10. Williams, Robert M. and Kenneth R. Reader. Two-Dimensional Subsonic Wind Tunnel Tests on a 50-Percent Thick Circulation Control Airfoil With Blowing Slots Located at 88.6 and 98.5 Percent Chord. (Naval Ship Research and Development Center, Tech. Note Al-186) (In preparation)

11. Tanner, Watson H. Charts for Estimating Rotary Wing Performance in Hover and at High Forward Speeds. Wash., Nov 1964, 146 p. (National Aeronautics and Space Administration Contactor Rpt. 114) (United Aircraft Corp. Contr NASW-745)

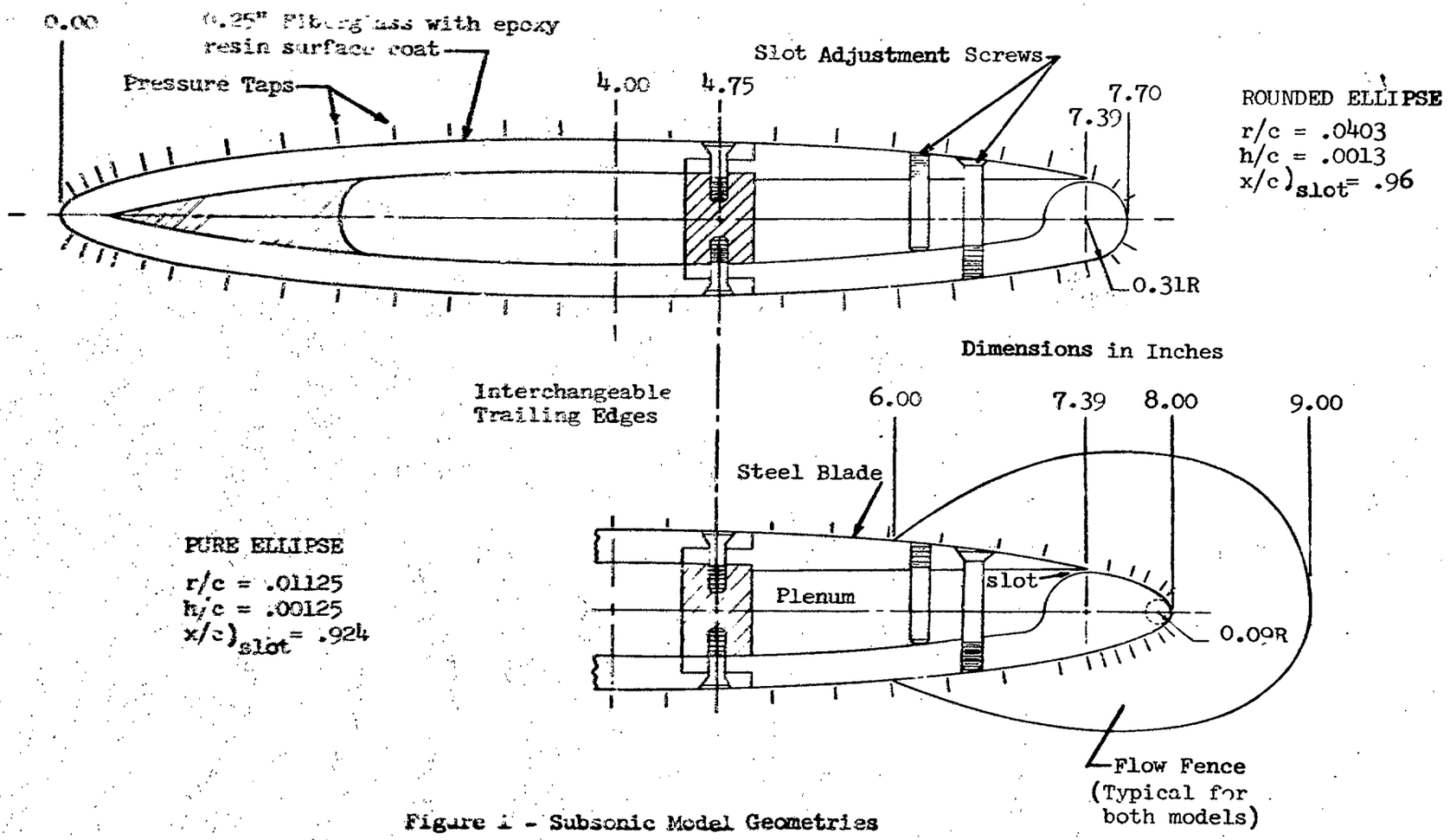

Figure 1 - Subsonic Model Geometries

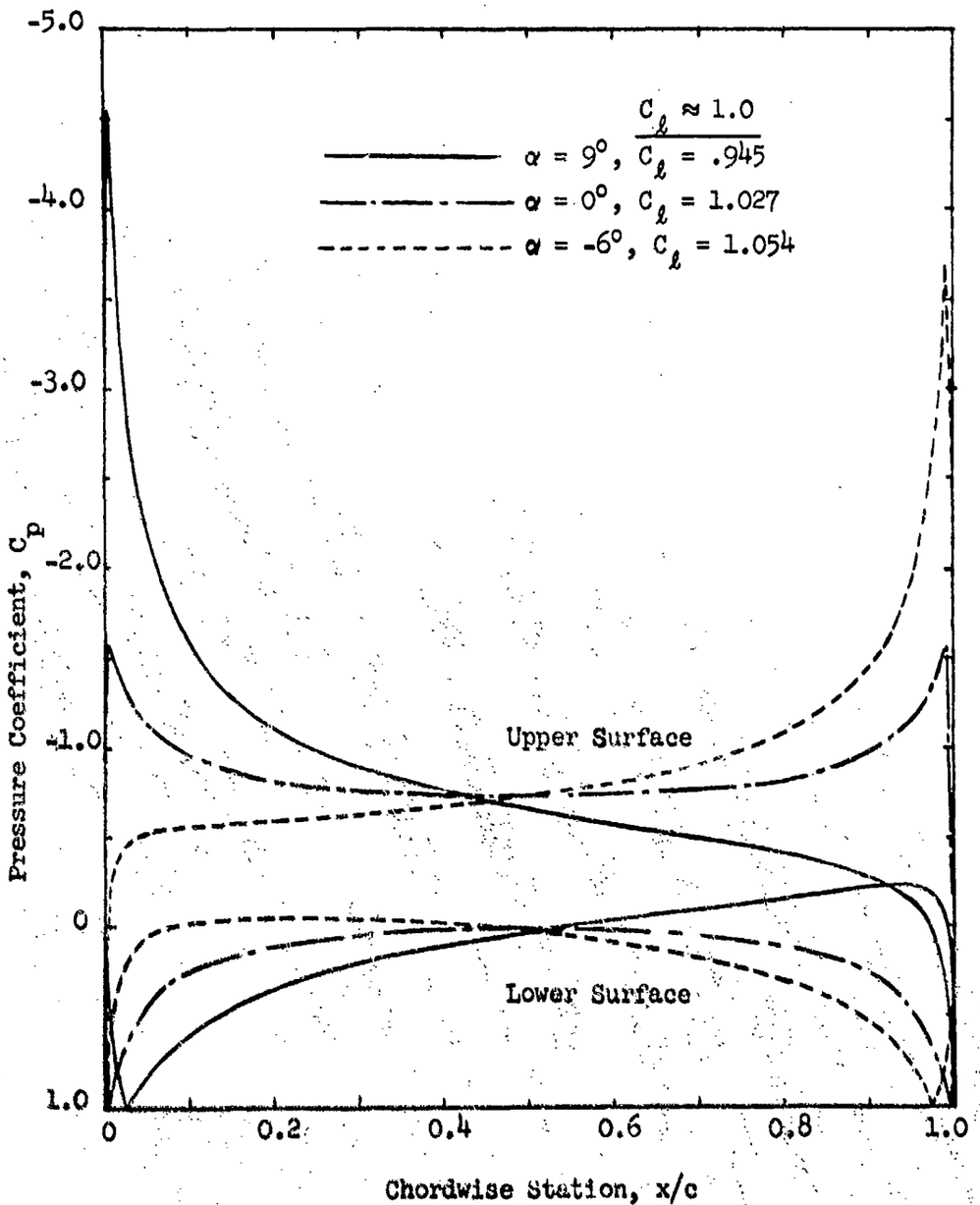

Figure 2 - Potential Flow Pressure Distributions on a 15 - Percent Pure Ellipse at Angle of Attack

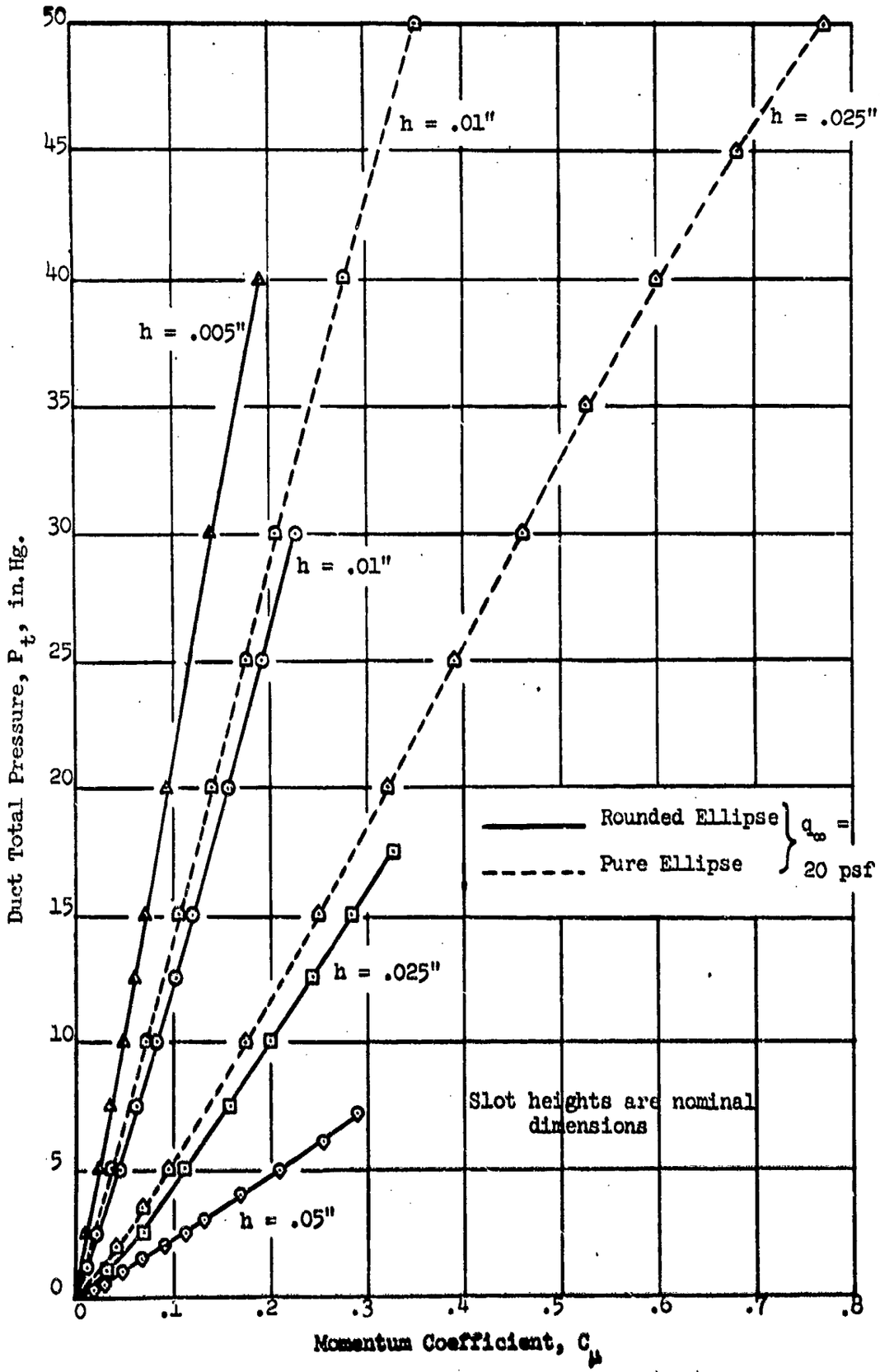

Figure 3 - Variation of Momentum Coefficient With Duct Pressure and Slot Height

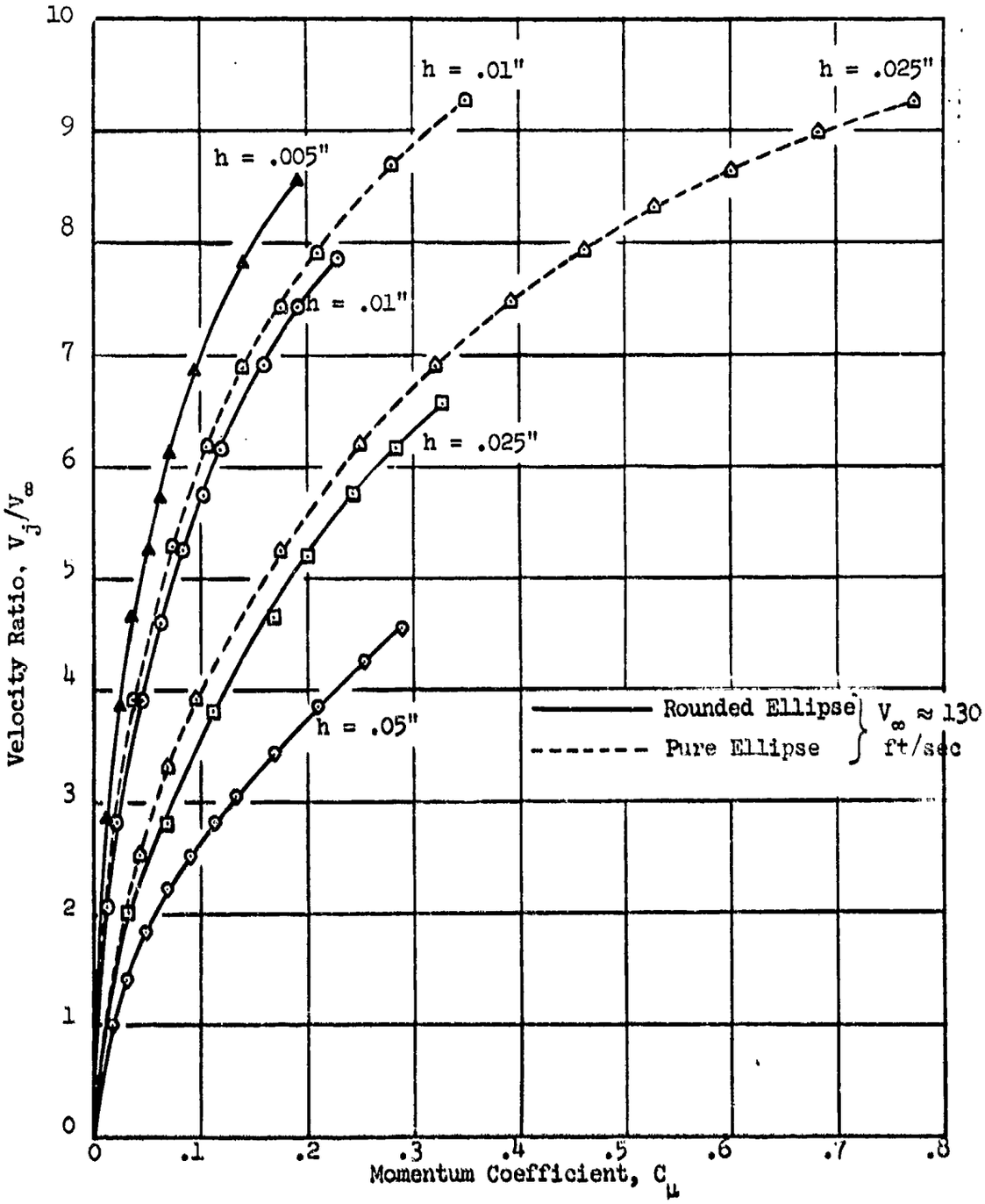

Figure 4 - Variation of Velocity Ratio with Momentum Coefficient and Slot Height

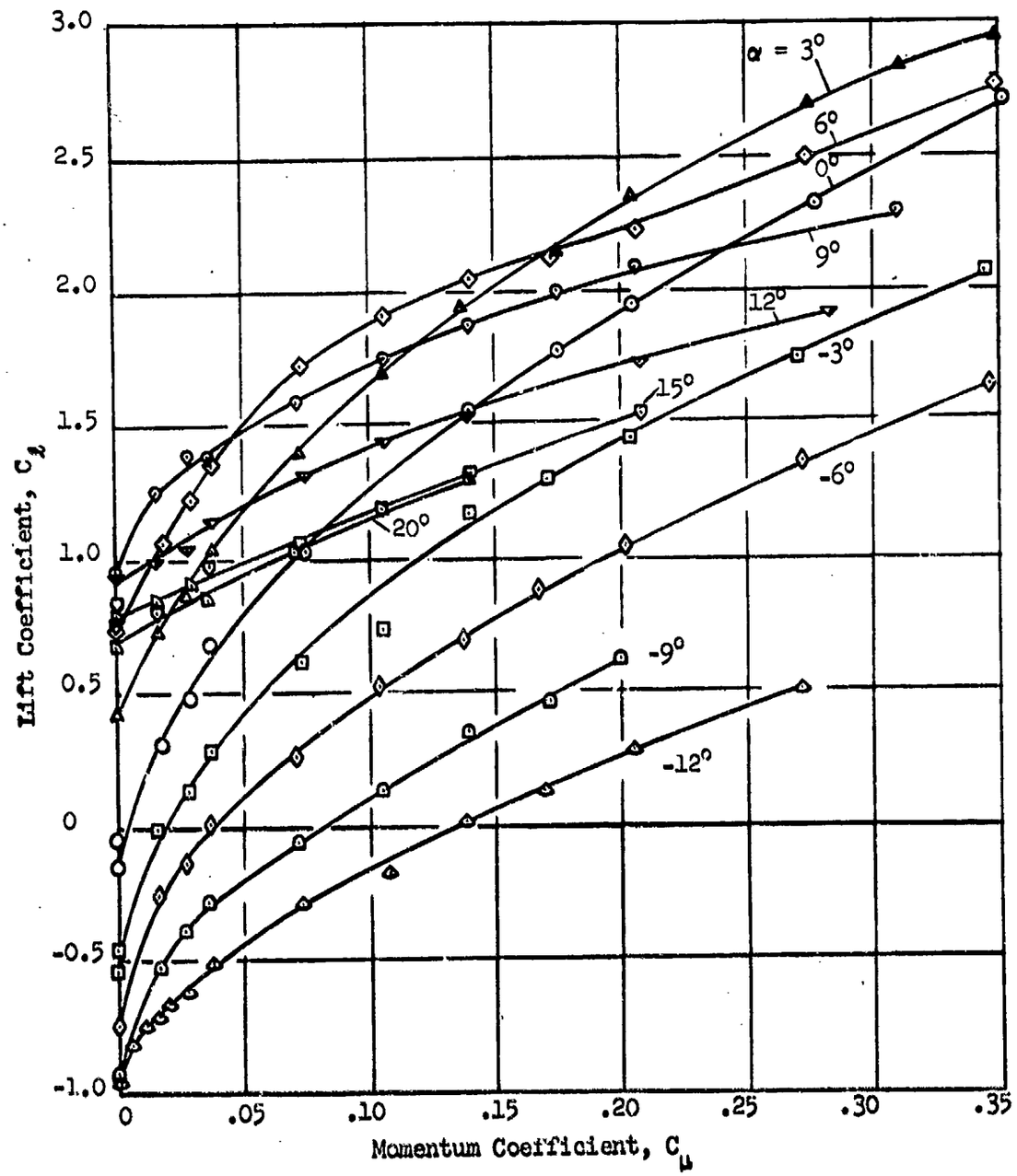

Figure 5 - Pure Ellipse Lift Variation with Momentum Coefficient, h = 0.01 inch

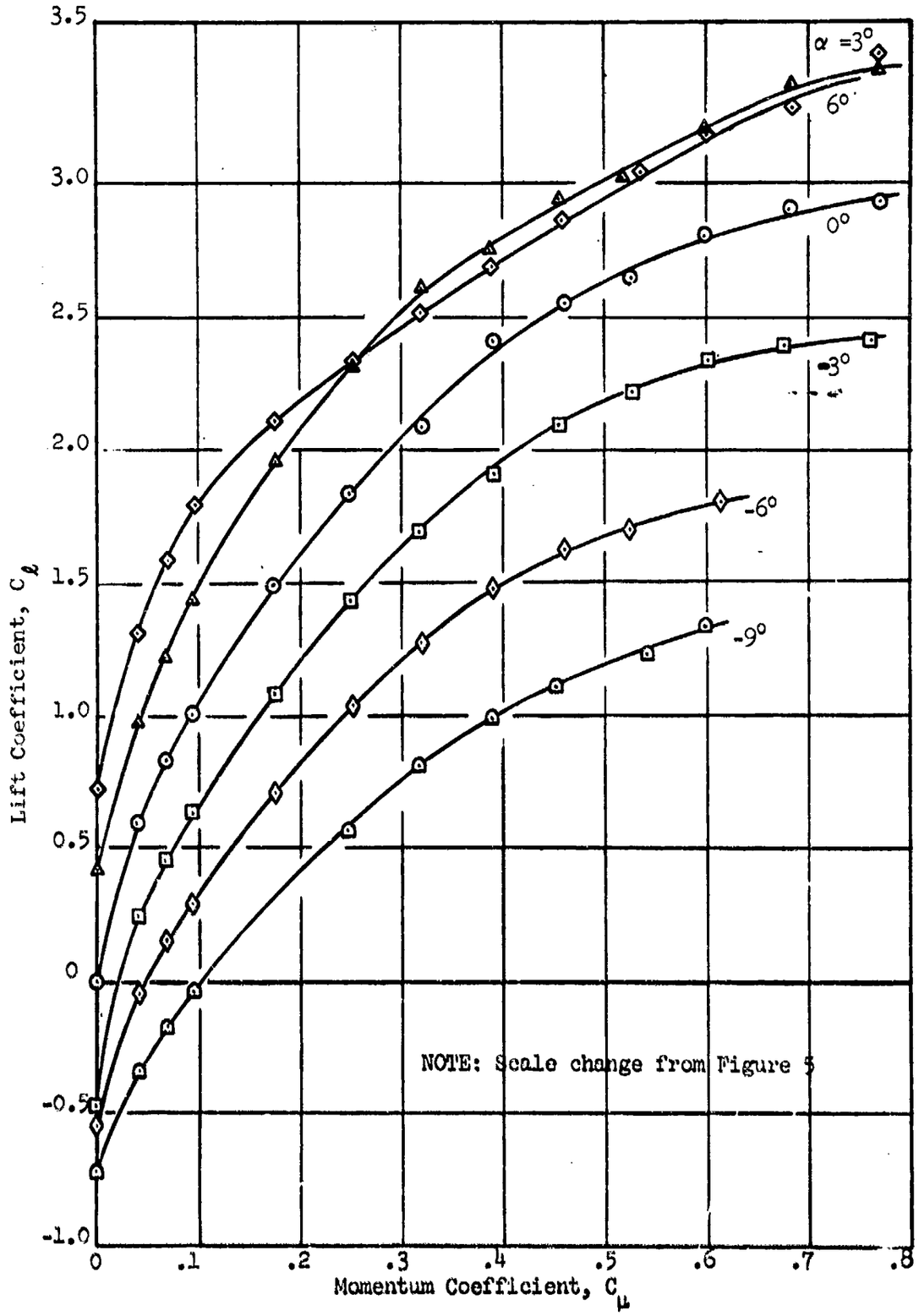

Figure 6 - Pure Ellipse Lift Variation With Momentum Coefficient, h = 0.025 inch

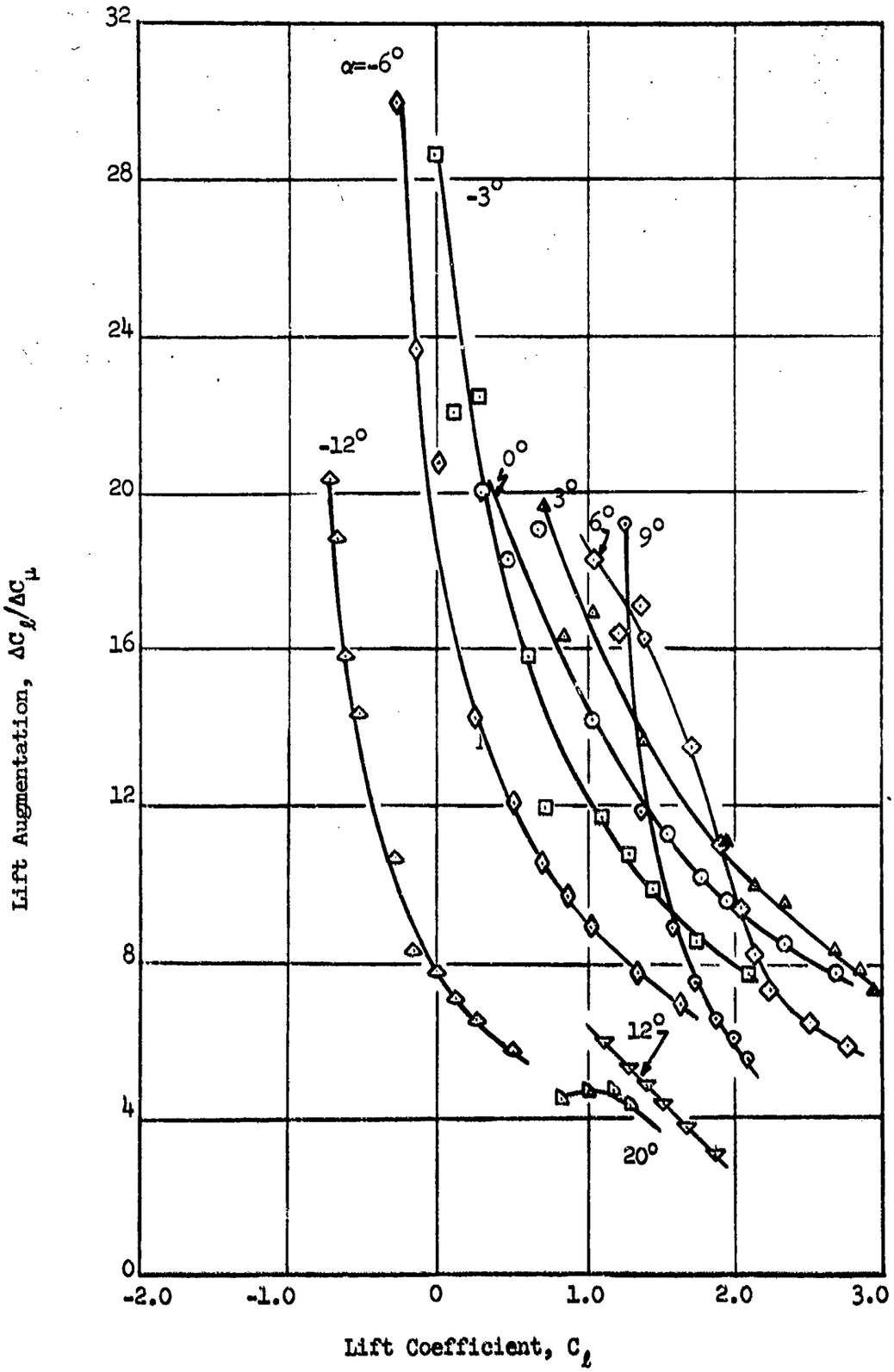

Figure 7 - Pure Ellipse Lift Augmentation, h = 0.01 inch

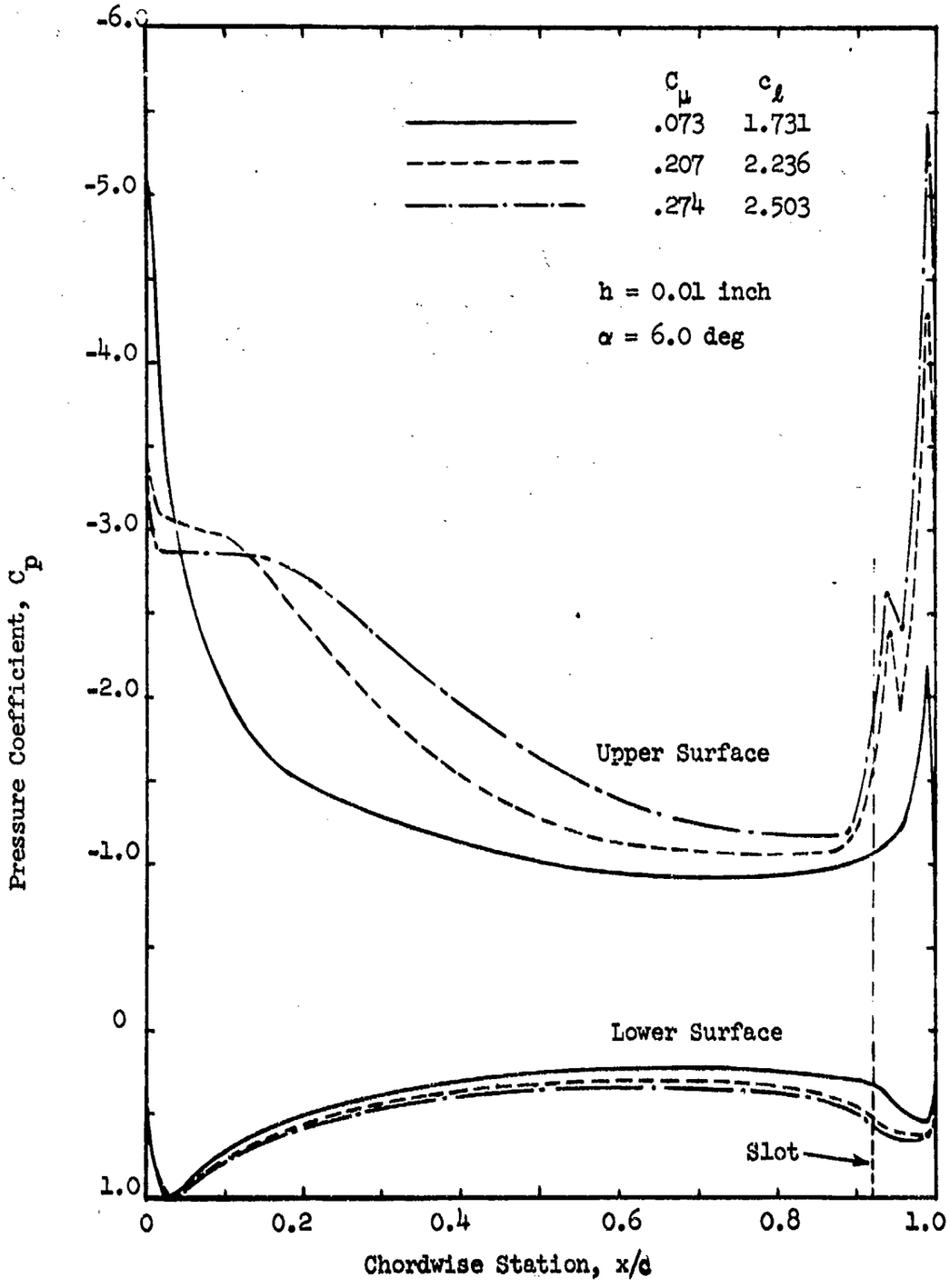

Figure 8 - Experimental Pressure Distributions for the Pure Ellipse Showing Leading Edge Bubble Formation

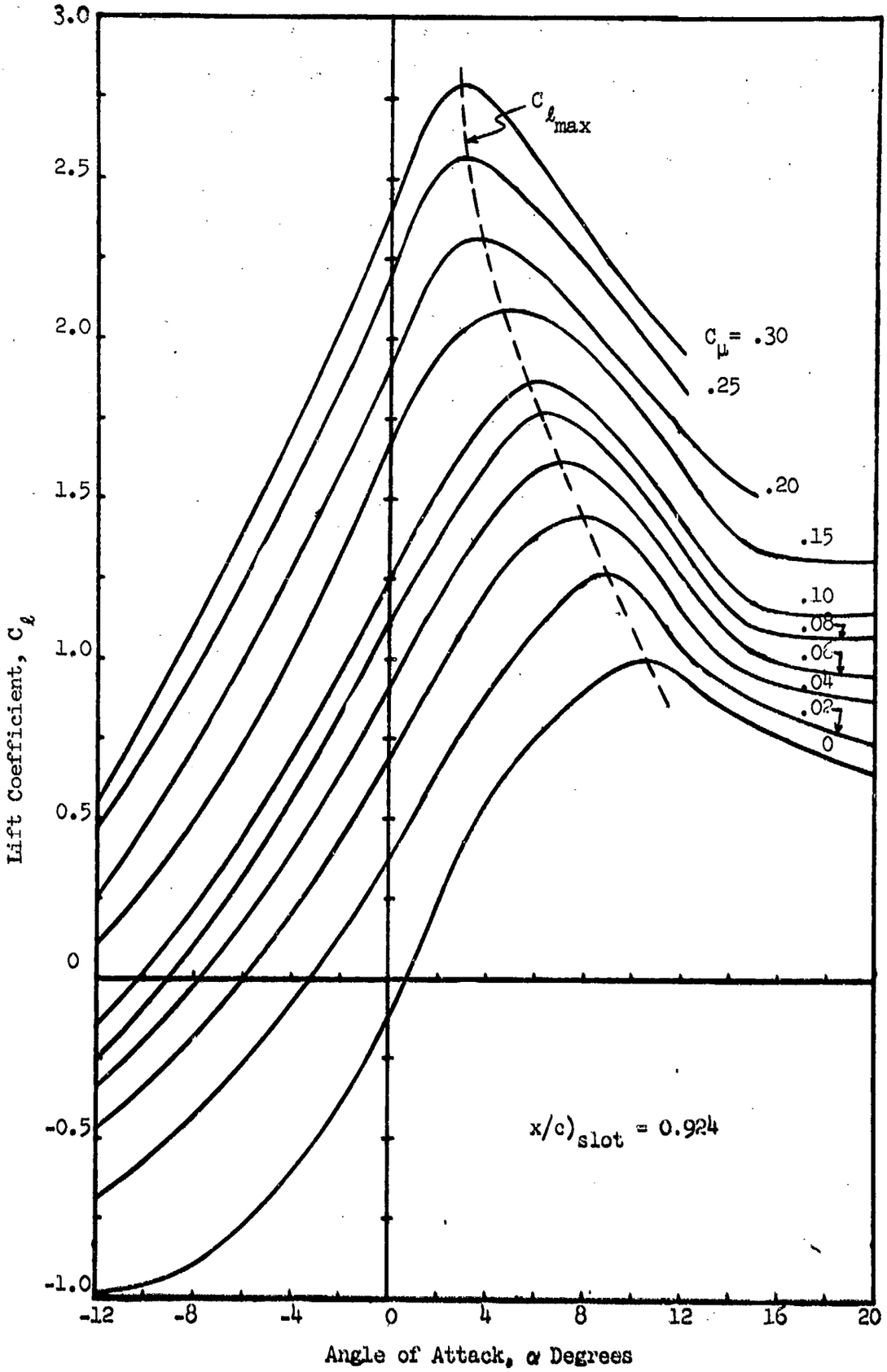

Figure 9 - Pure Ellipse Lift Variation with Angle of Attack, h = 0.01 inch

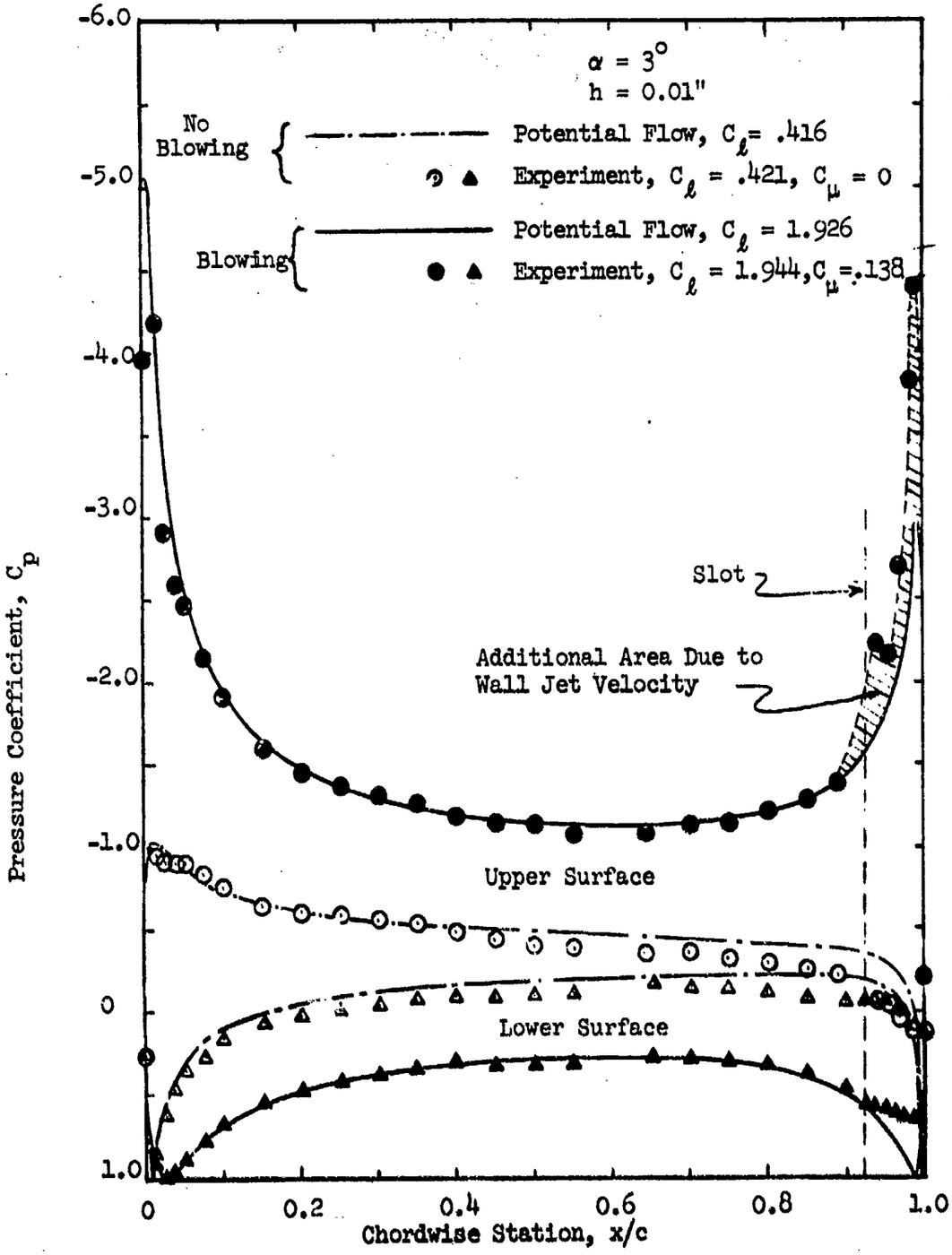

Figure 10 - Comparison Between Potential Flow and Experimental Pressure Distributions for the Pure Ellipse

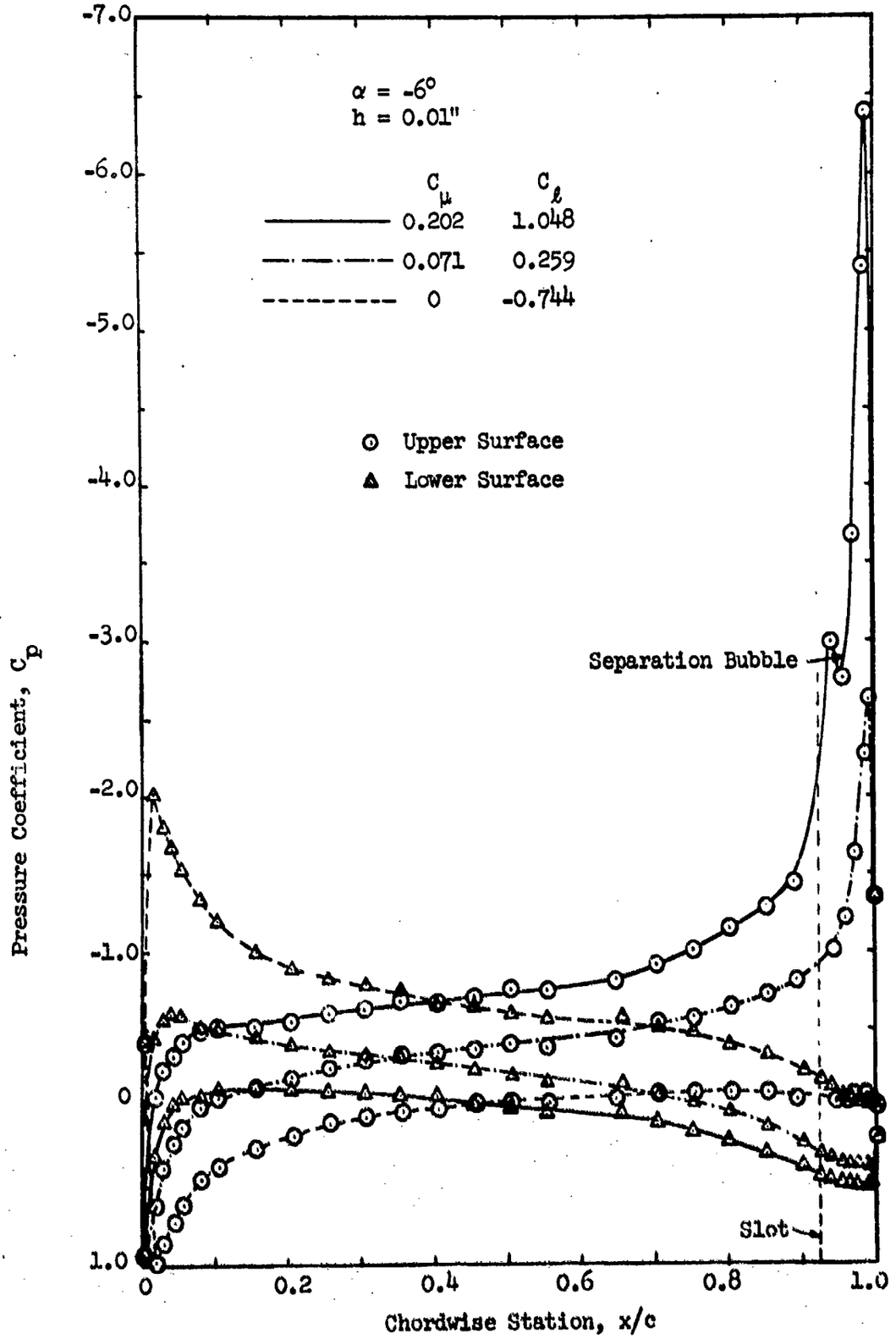

Figure 11 - Pure Ellipse Pressure Distributions at Negative Angle of Attack

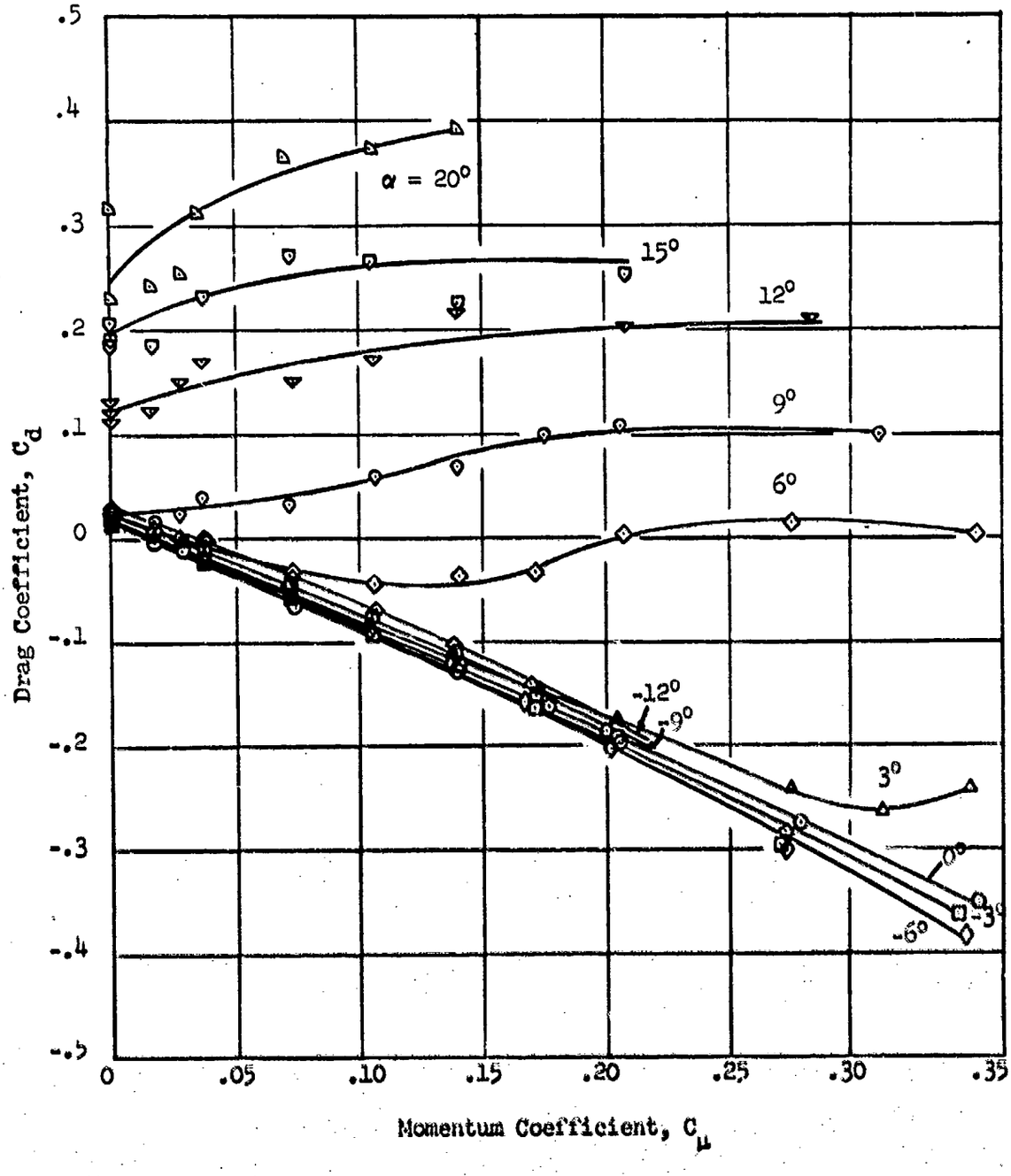

Figure 12 - Drag Coefficient Variation with Momentum Coefficient for the Pure Ellipse, h = 0.01 inch

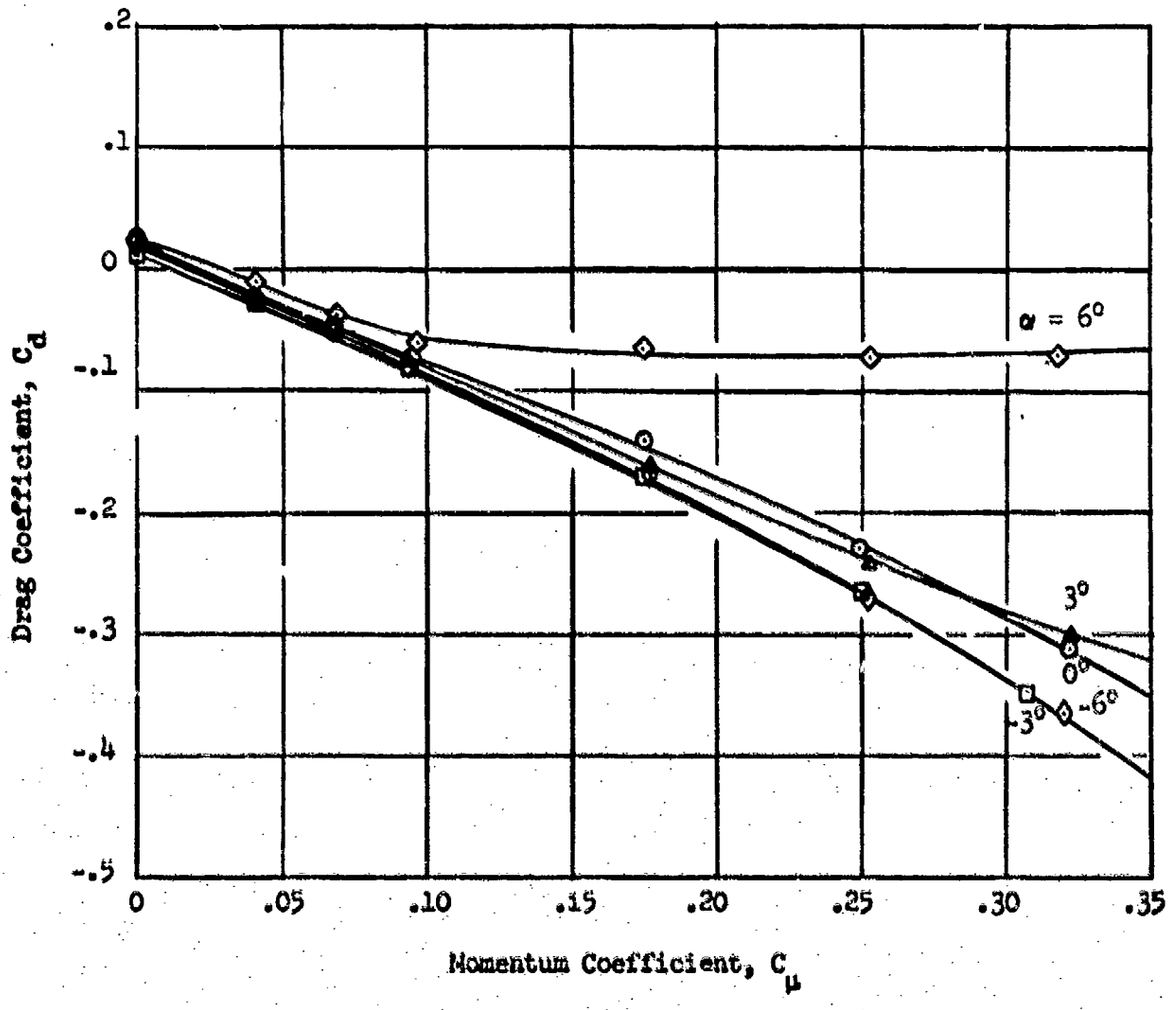

Figure 13 - Drag Coefficient Variation with Momentum Coefficient for the Pure Ellipse, h = 0.025 inch

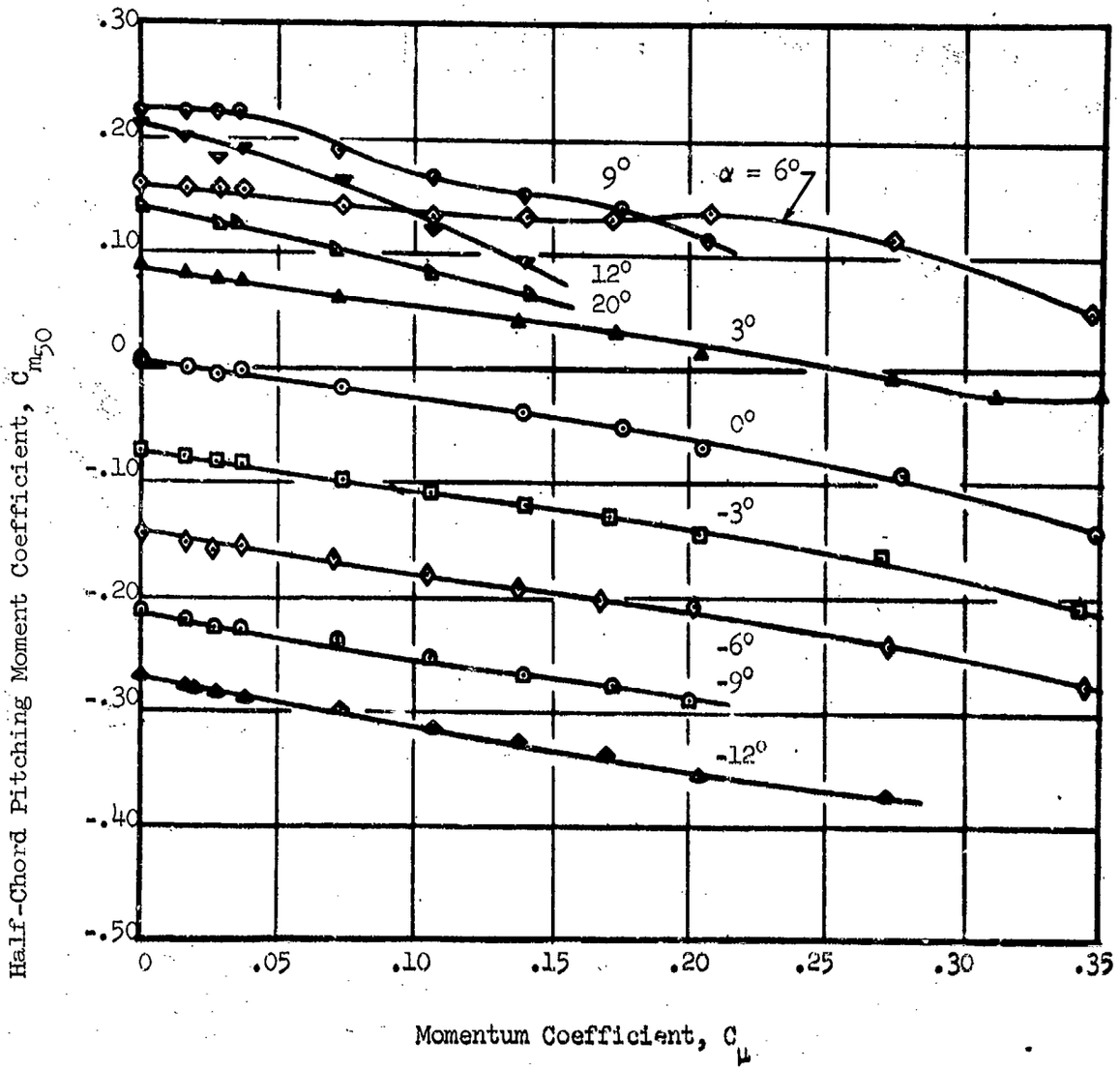

Figure 14 - Variation in Half-Chord Pitching Moment Coefficient for the Pure Ellipse, h = 0.01 inch

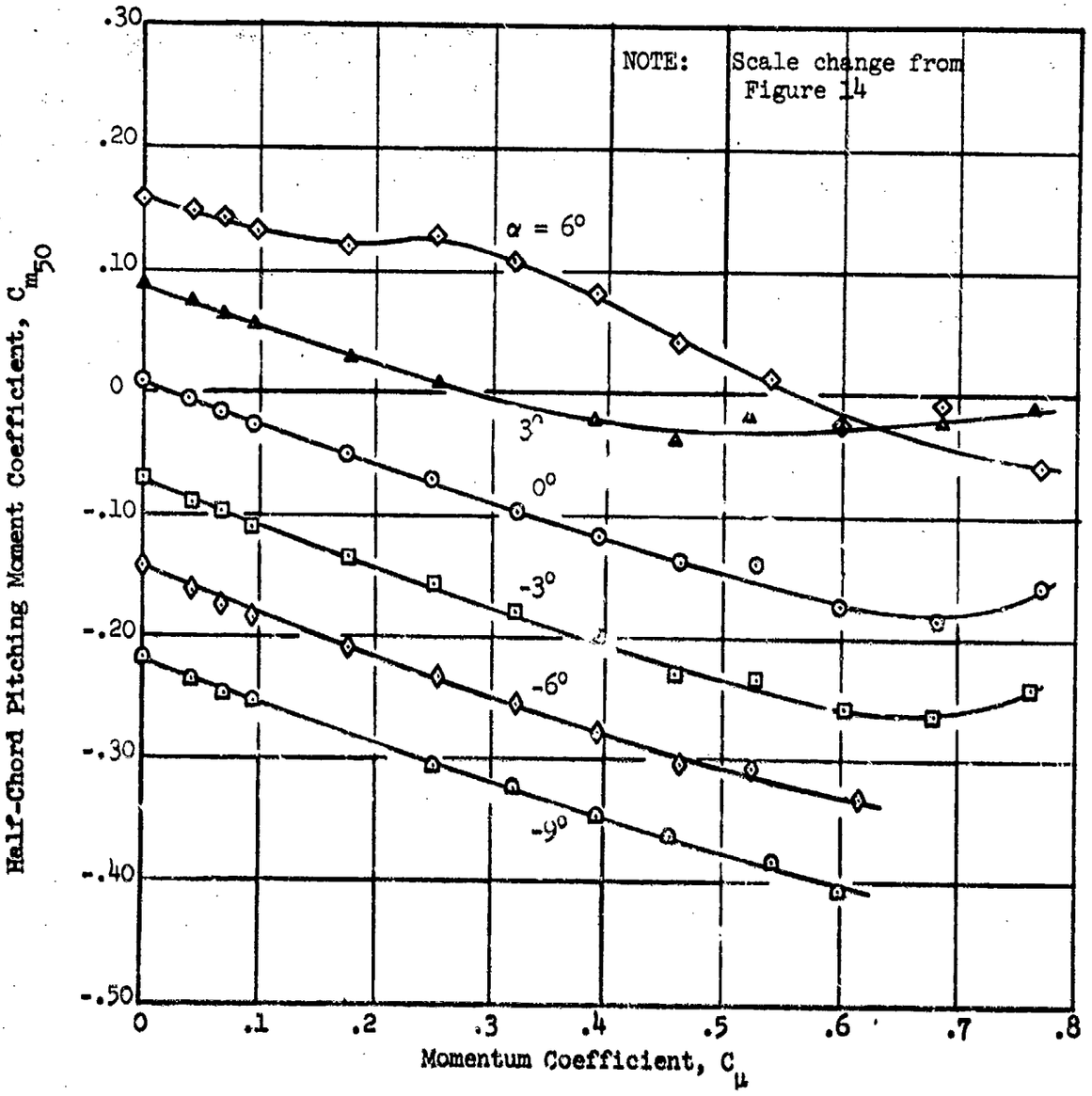

Figure 15 - Variation in Half-Chord Pitching Moment Coefficient for the Pure Ellipse, h = 0.025 inch

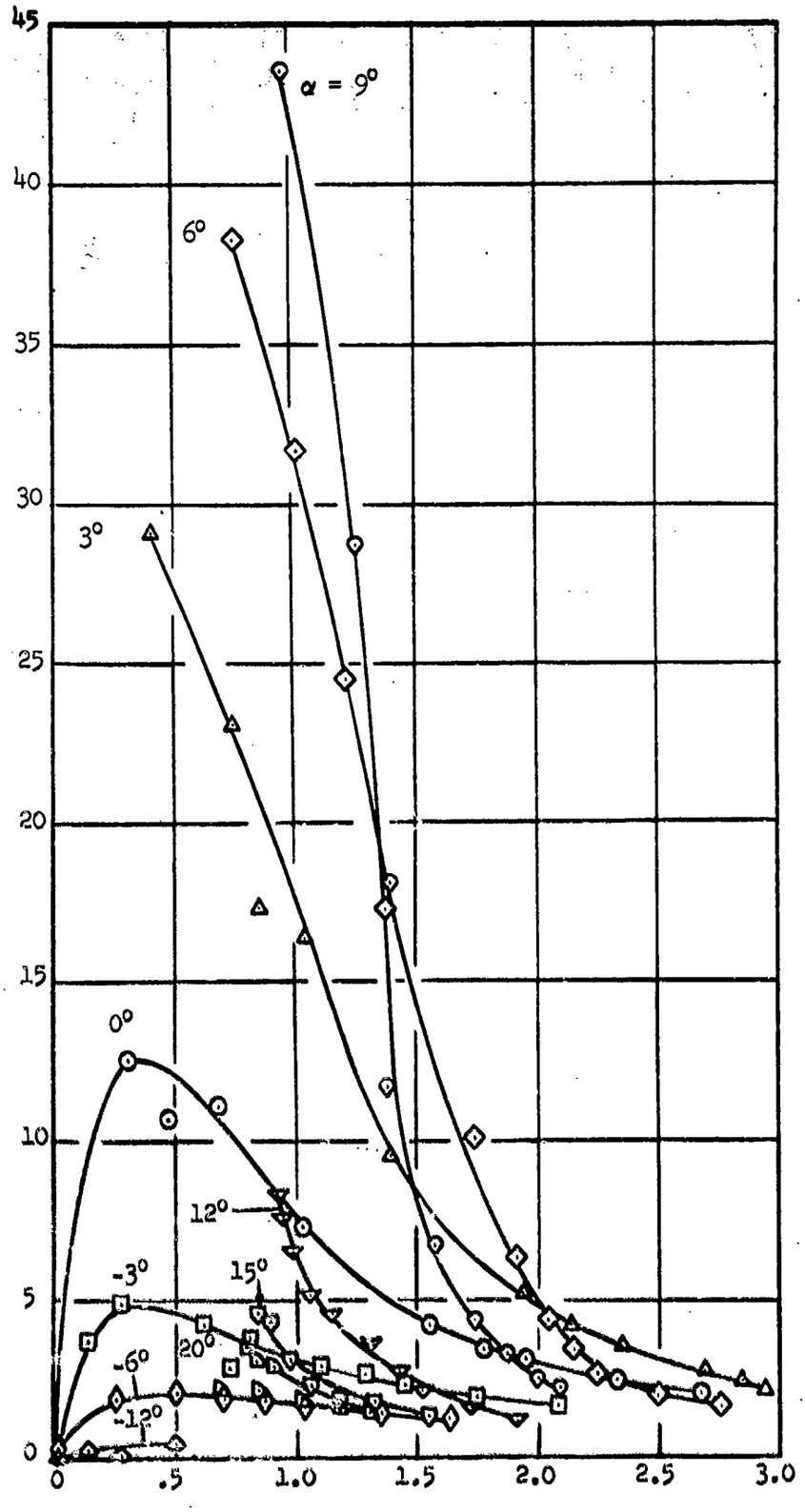

Figure 16 - Equivalent Lift-Drag Ratio for the Pure Ellipse, h = 0.01 inch

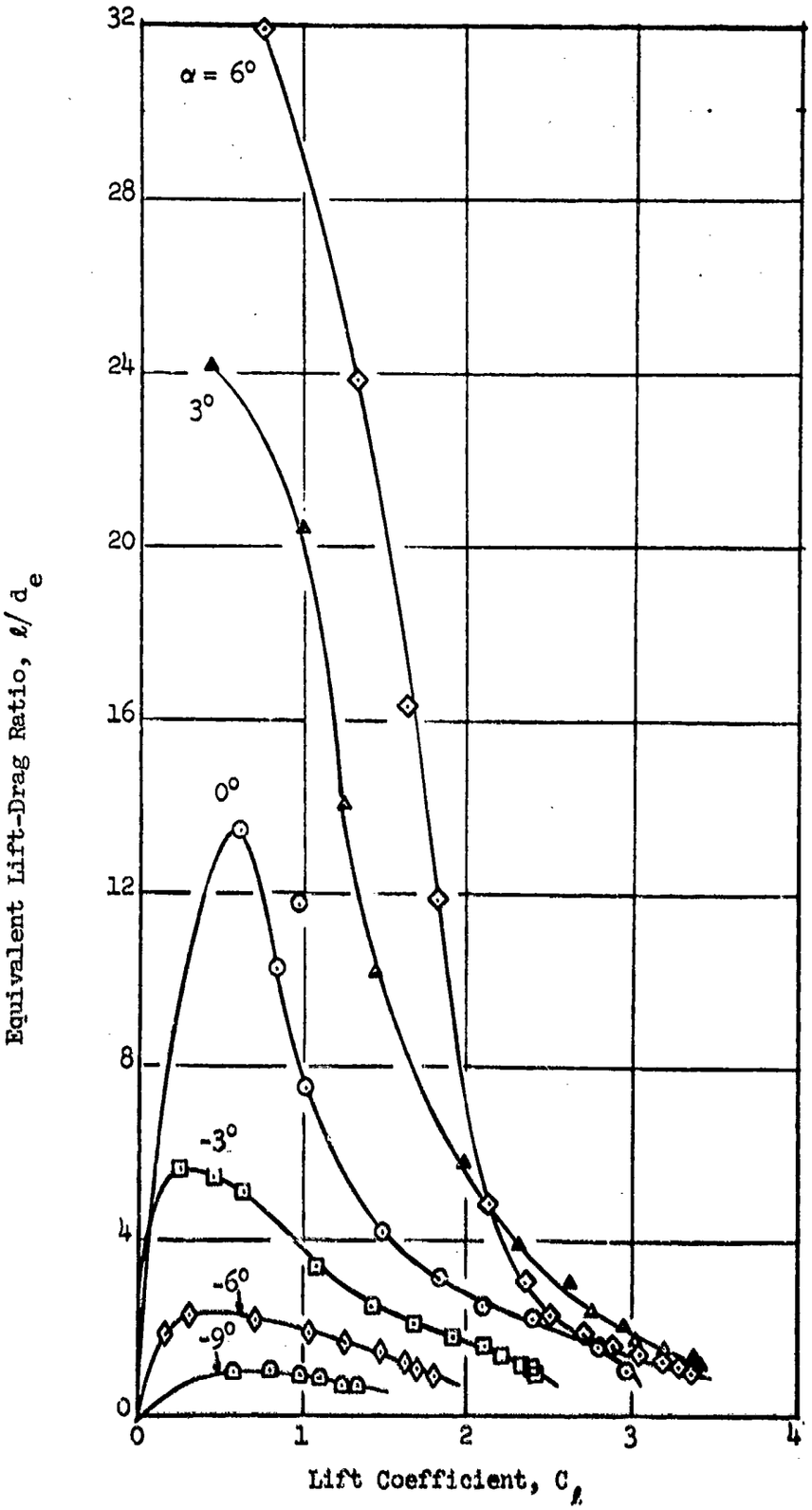

Figure 17 - Equivalent Lift-Drag Ratio for the Pure Ellipse, h = 0.025 inch

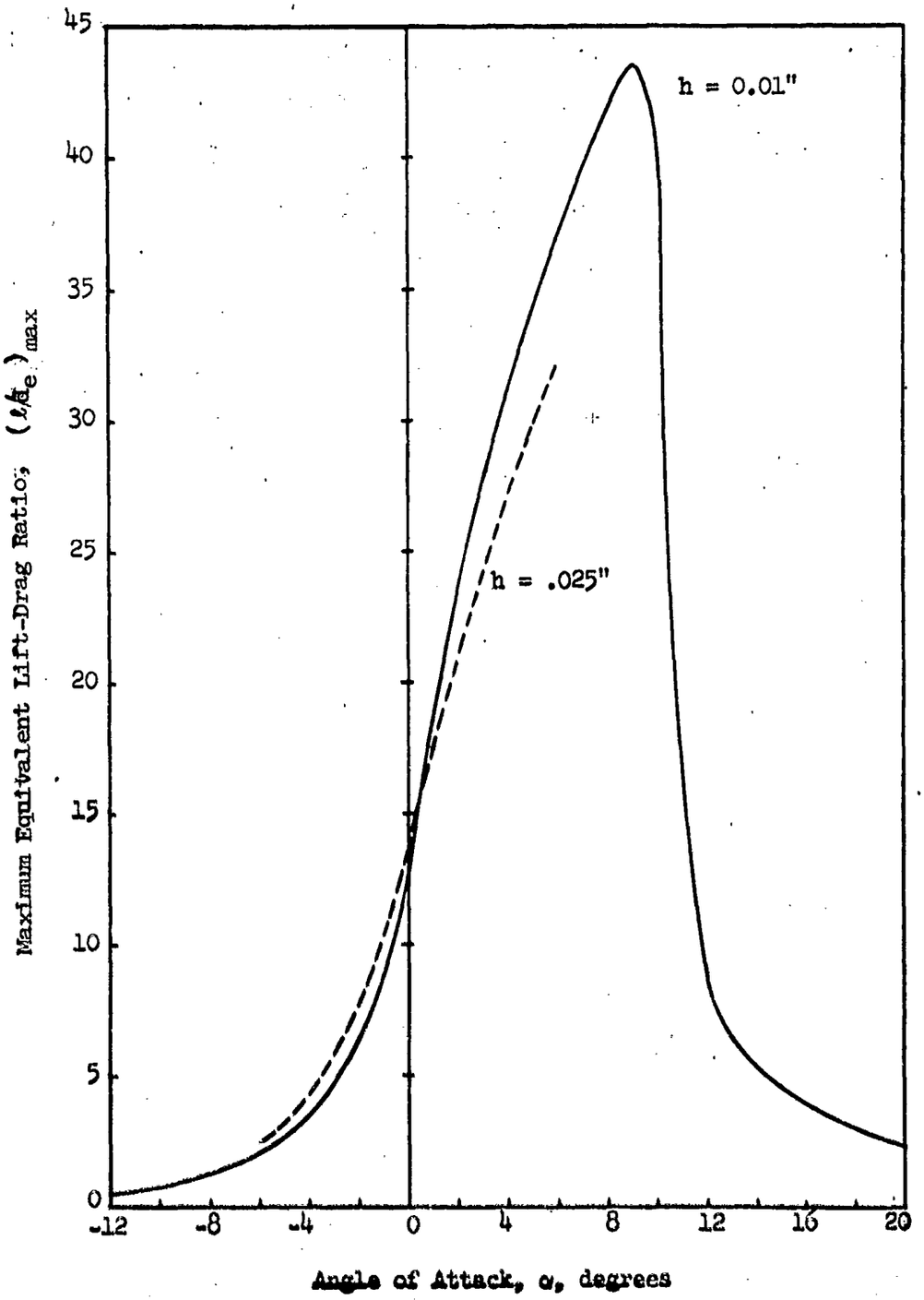

Figure 18 - Maximum Equivalent Lift-Drag Ratios for the Pure Ellipse

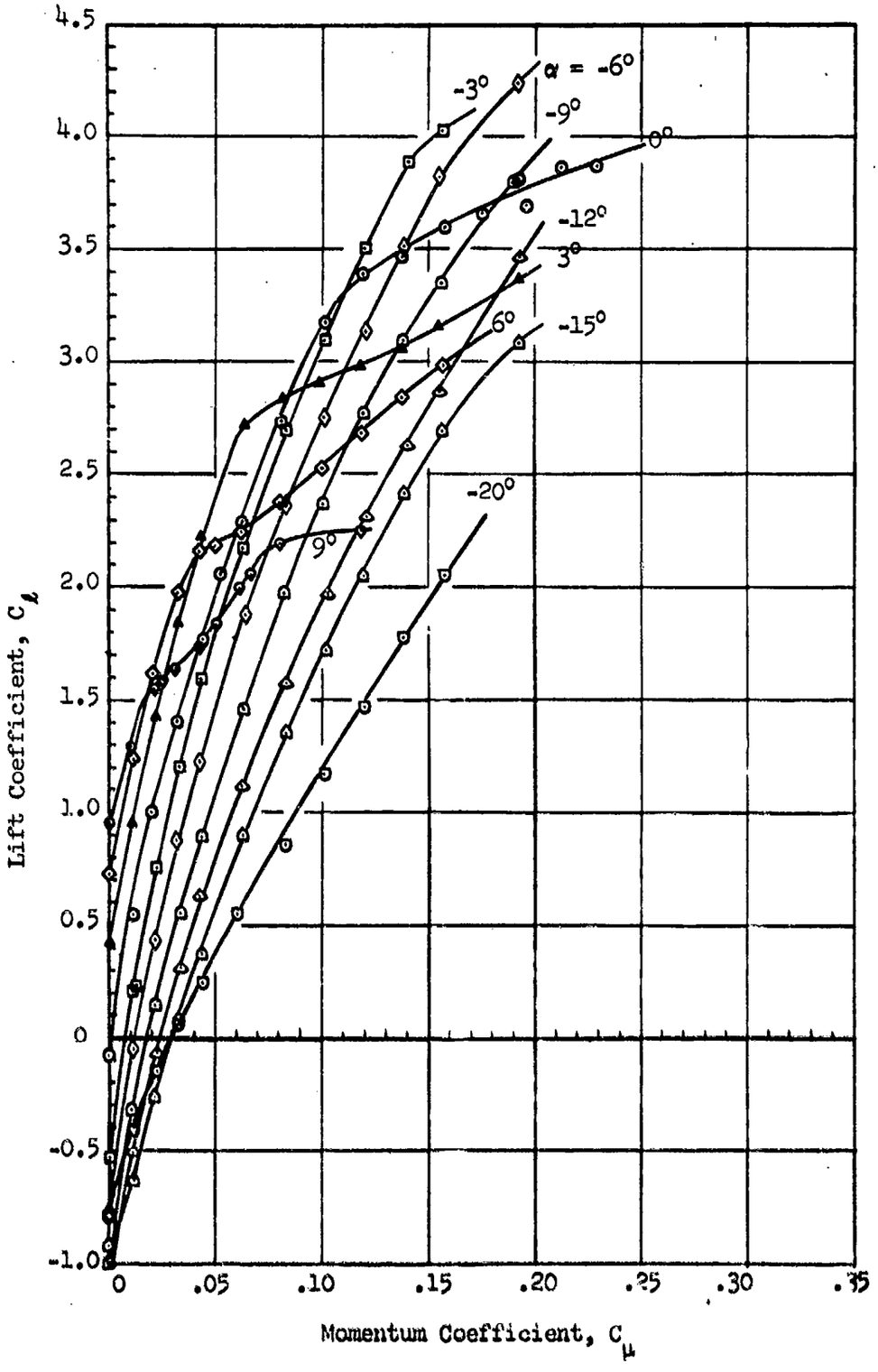

Figure 19 - Lift Variation with Momentum Coefficient for the Rounded Ellipse, h = 0.01 inch.

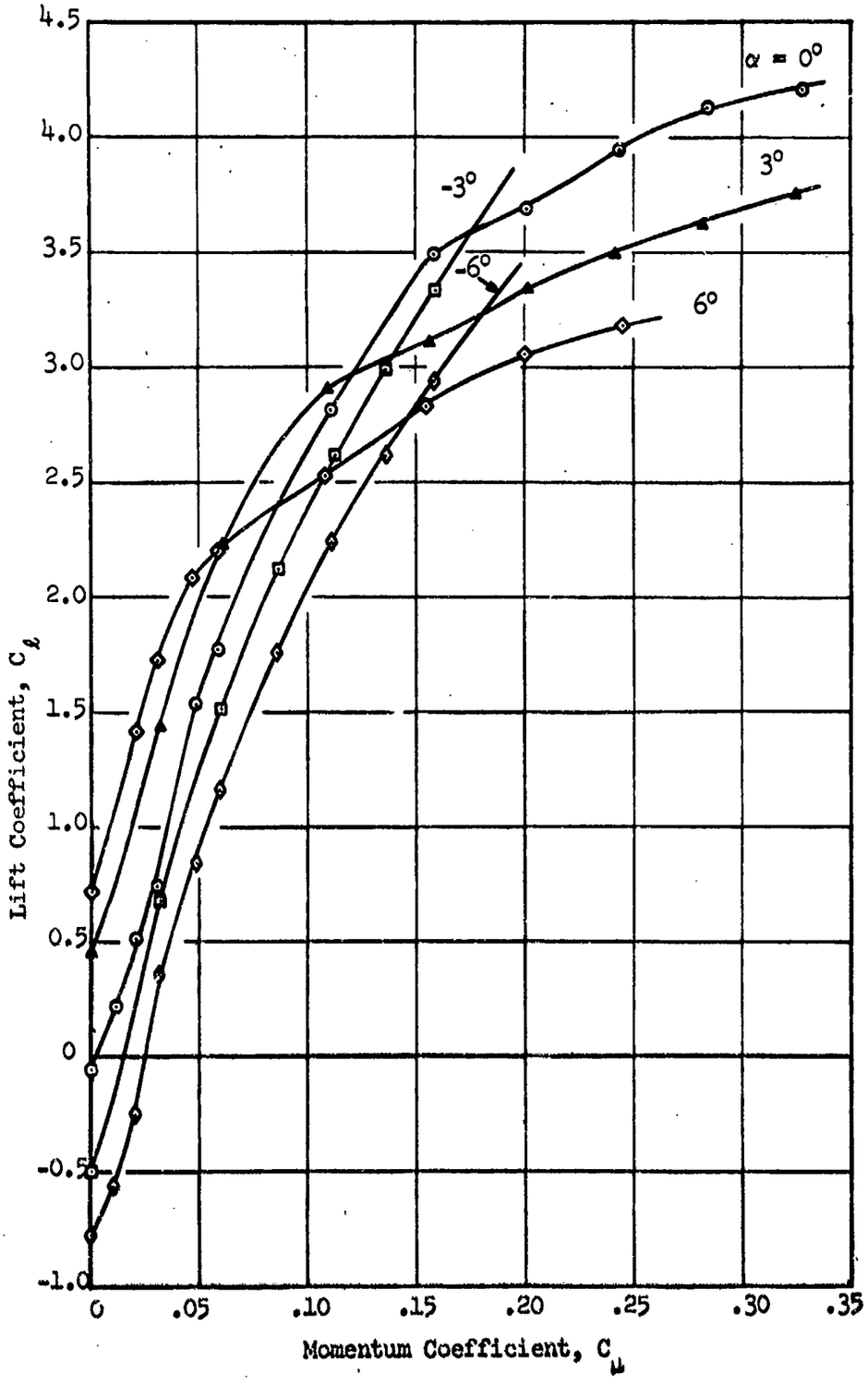

Figure 20 - Lift Variation with Momentum Coefficient for the Rounded Ellipse, h = 0.025 inch.

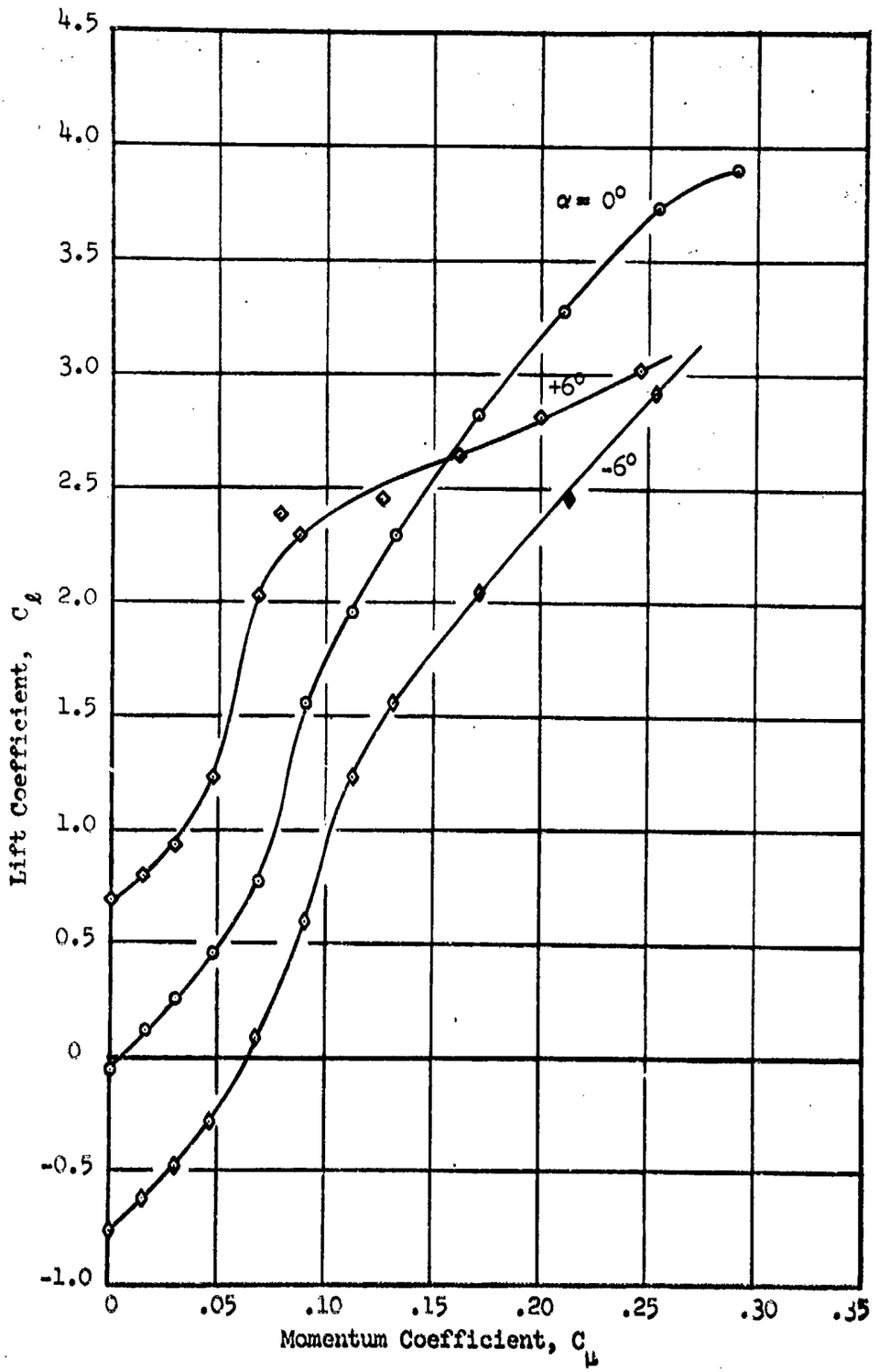

Figure 21 - Lift Variation with Momentum Coefficient for the Rounded Ellipse, h = 0.05 inch

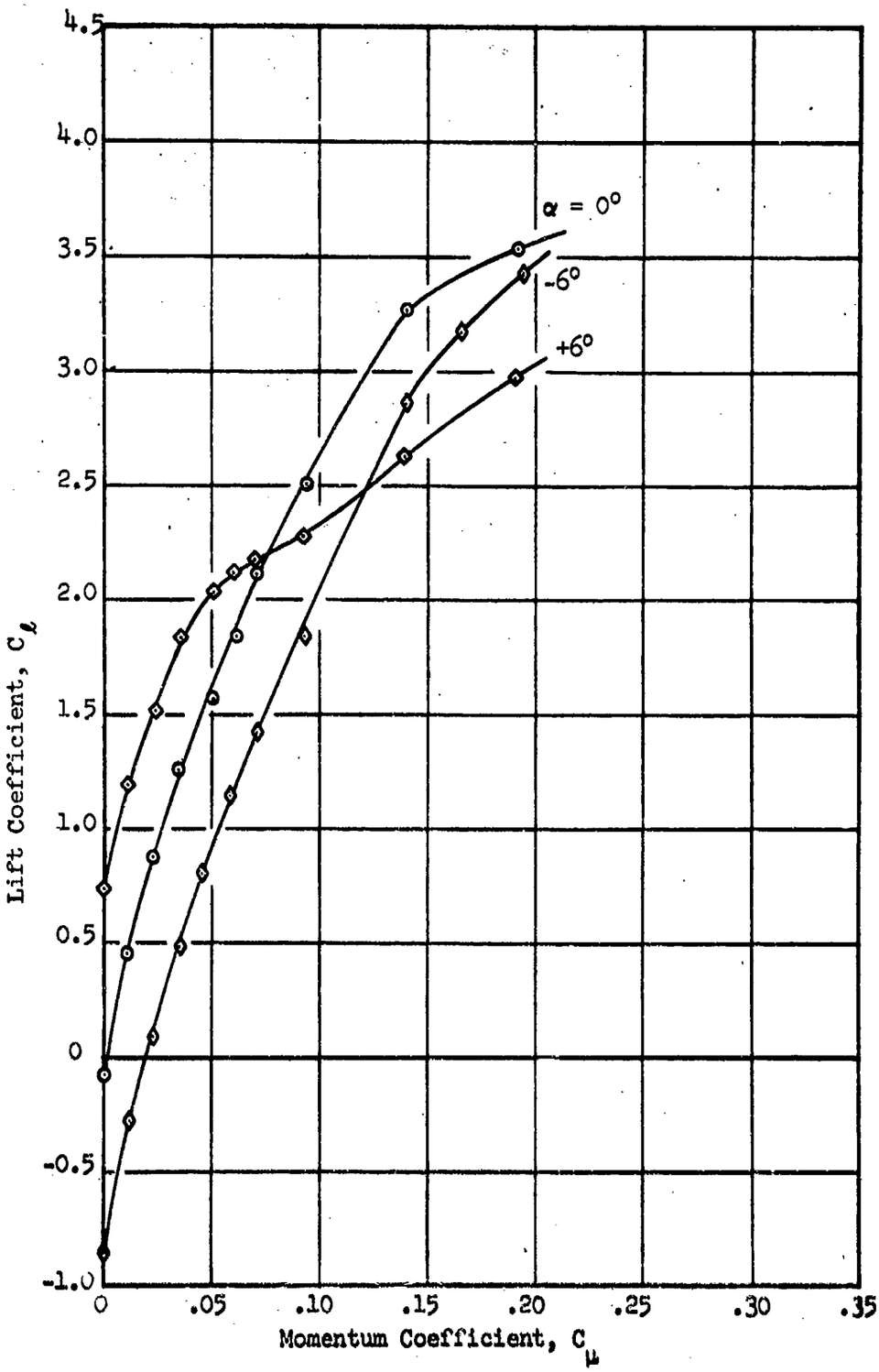

Figure 22 - Lift Variation with Momentum Coefficient for the Rounded Ellipse, h = 0.005 inch

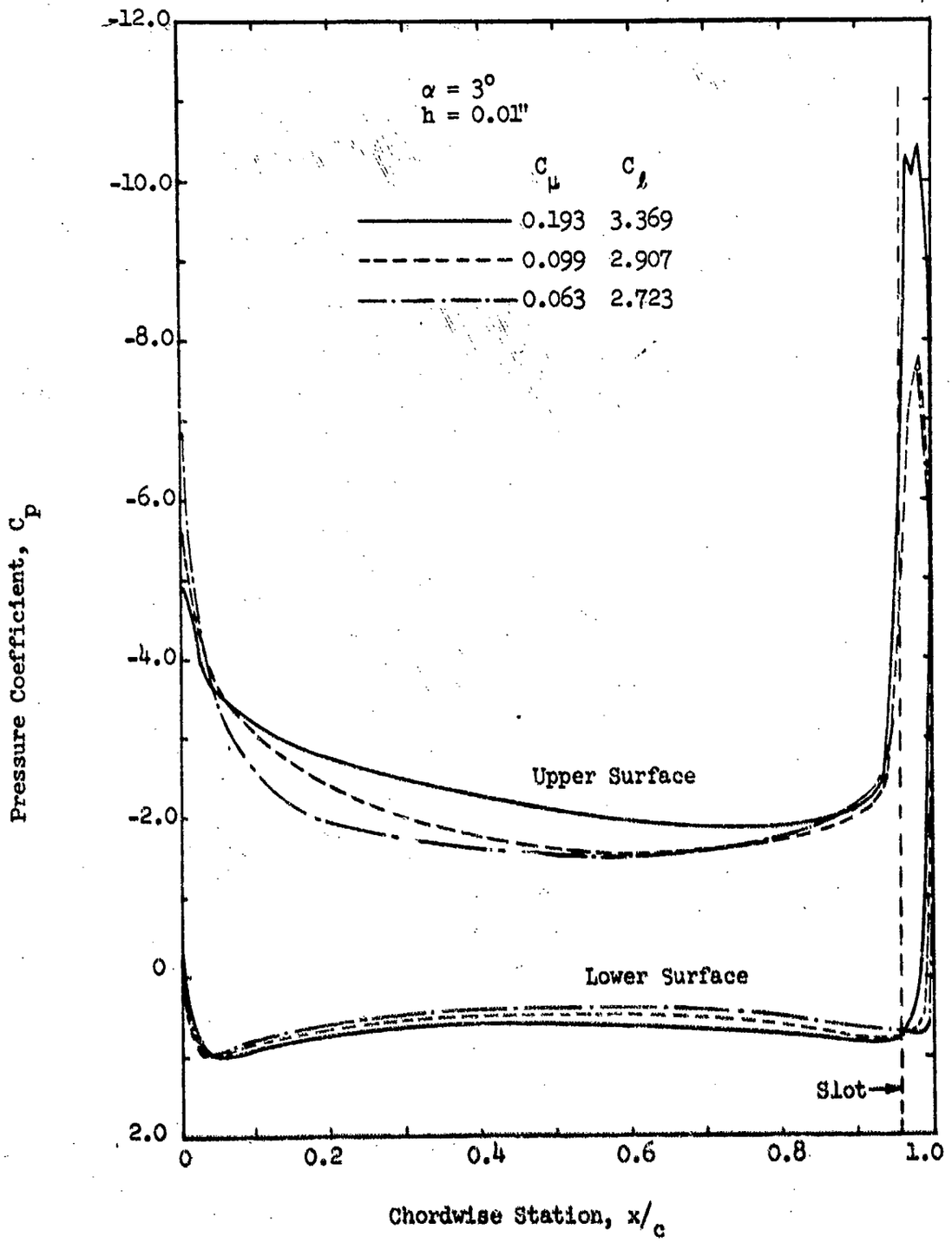

Figure 23 - Rounded Ellipse Experimental Pressure Distributions Showing Leading Edge Suction Loss

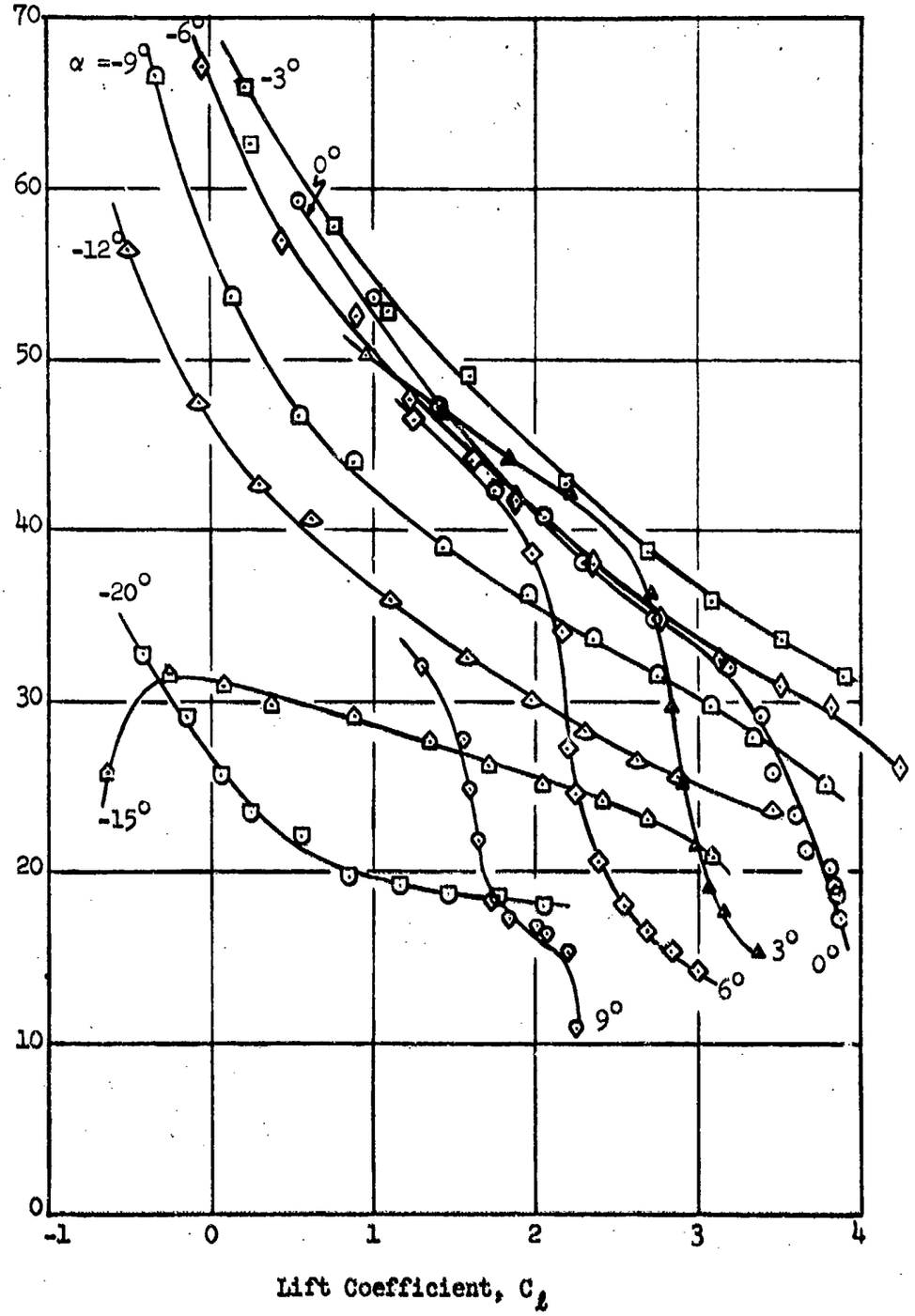

Figure 24 - Lift Augmentation for the Rounded Ellipse, h = 0.01 inch

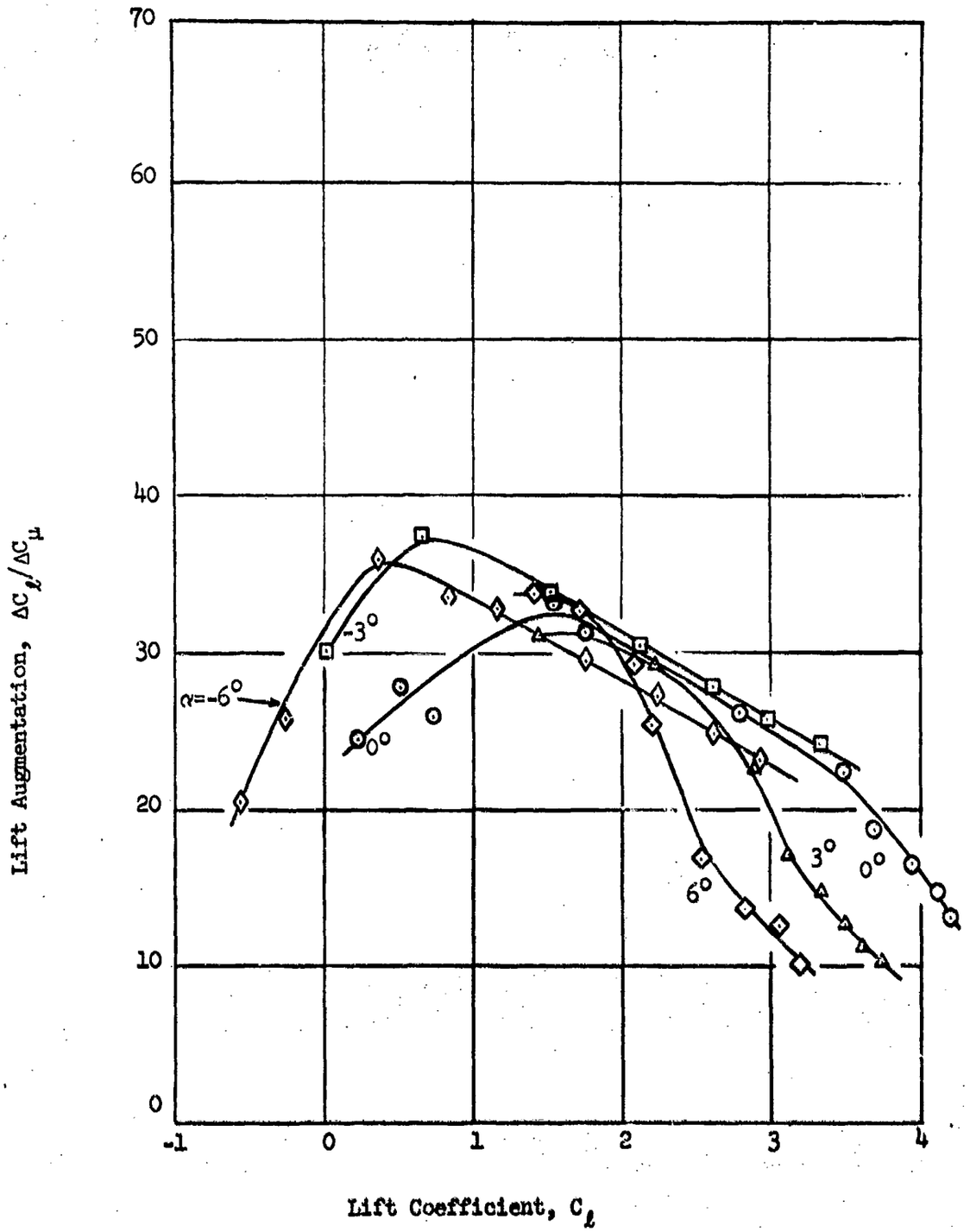

Figure 25 - Lift Augmentation for the Rounded Ellipse, h = 0.025 inch

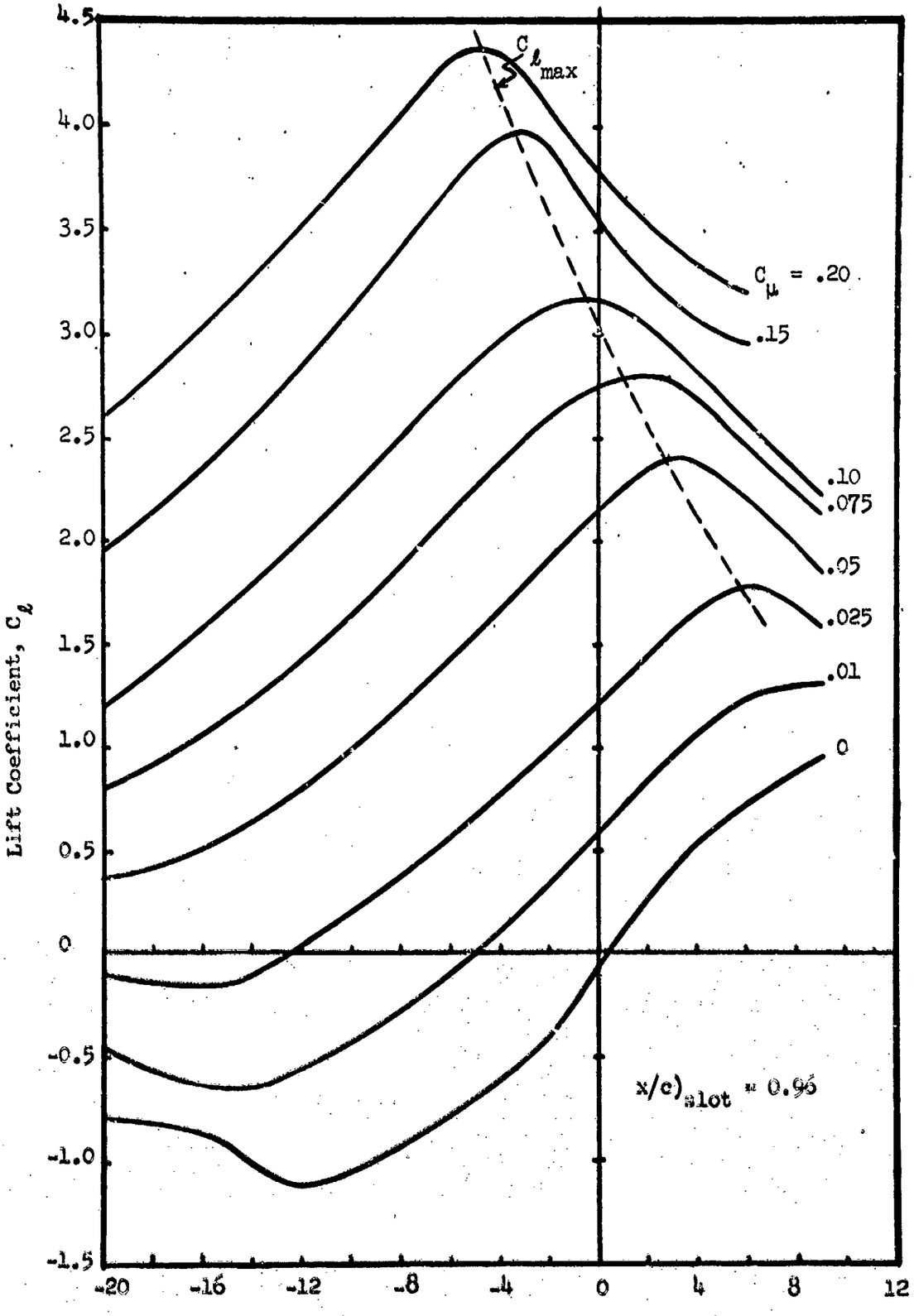

Figure 26 - Rounded Ellipse Lift Variation with Angle of Attack, h = 0.01 inch

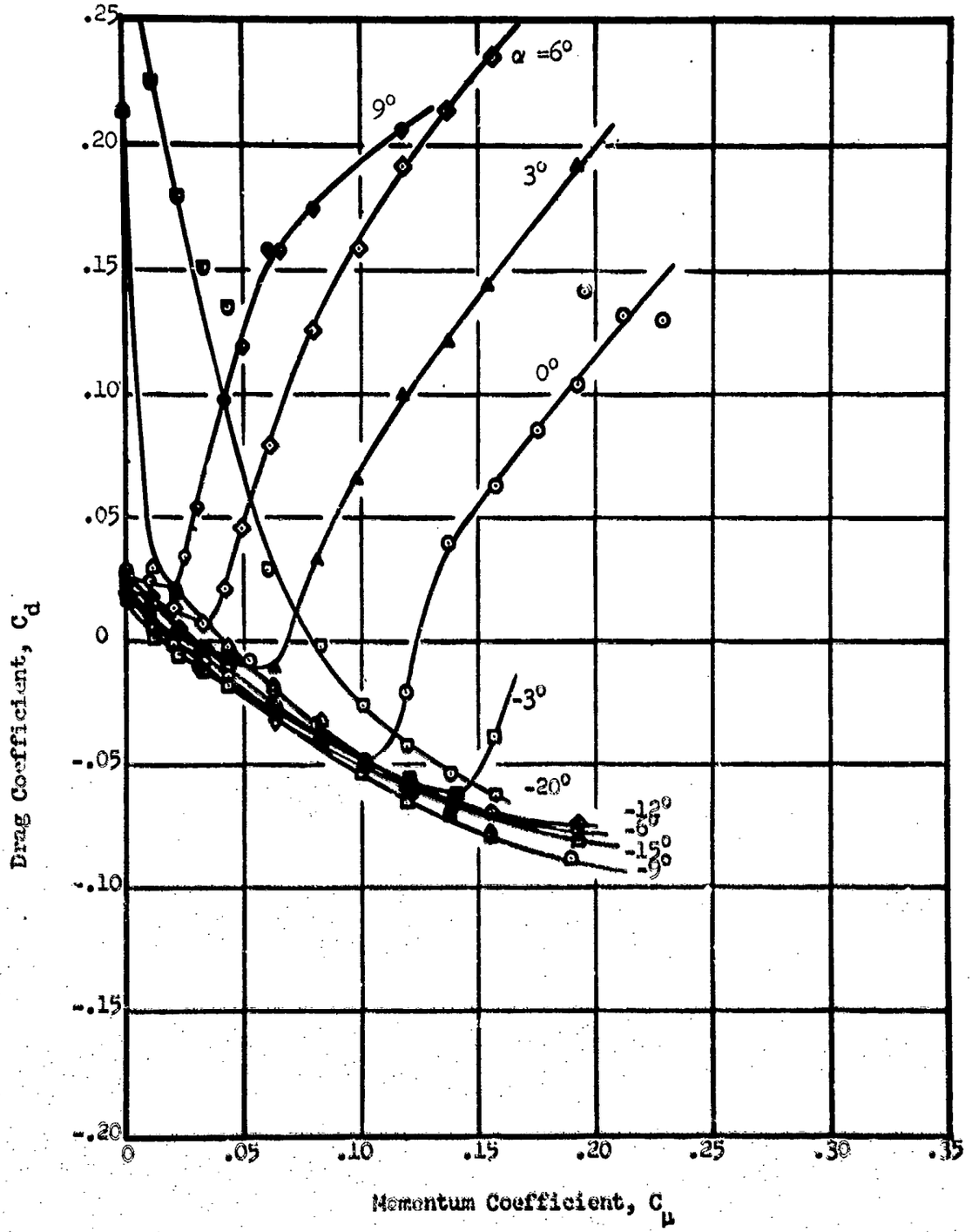

Figure 27 - Variation in Drag Coefficient for the Rounded Ellipse, h = 0.01 inch

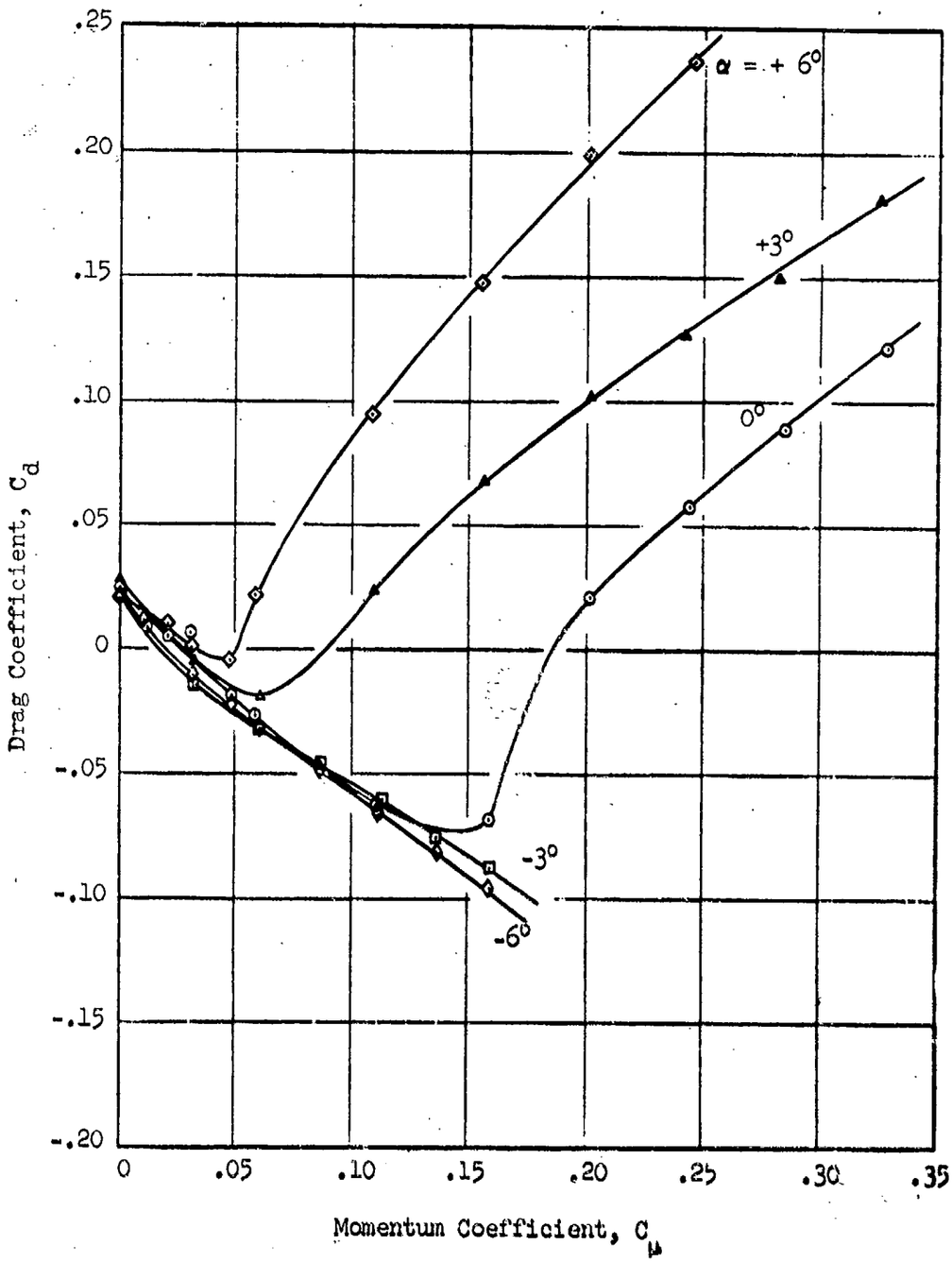

Figure 28 - Variation in Drag Coefficient for the Rounded Ellipse, h = 0.025 inch

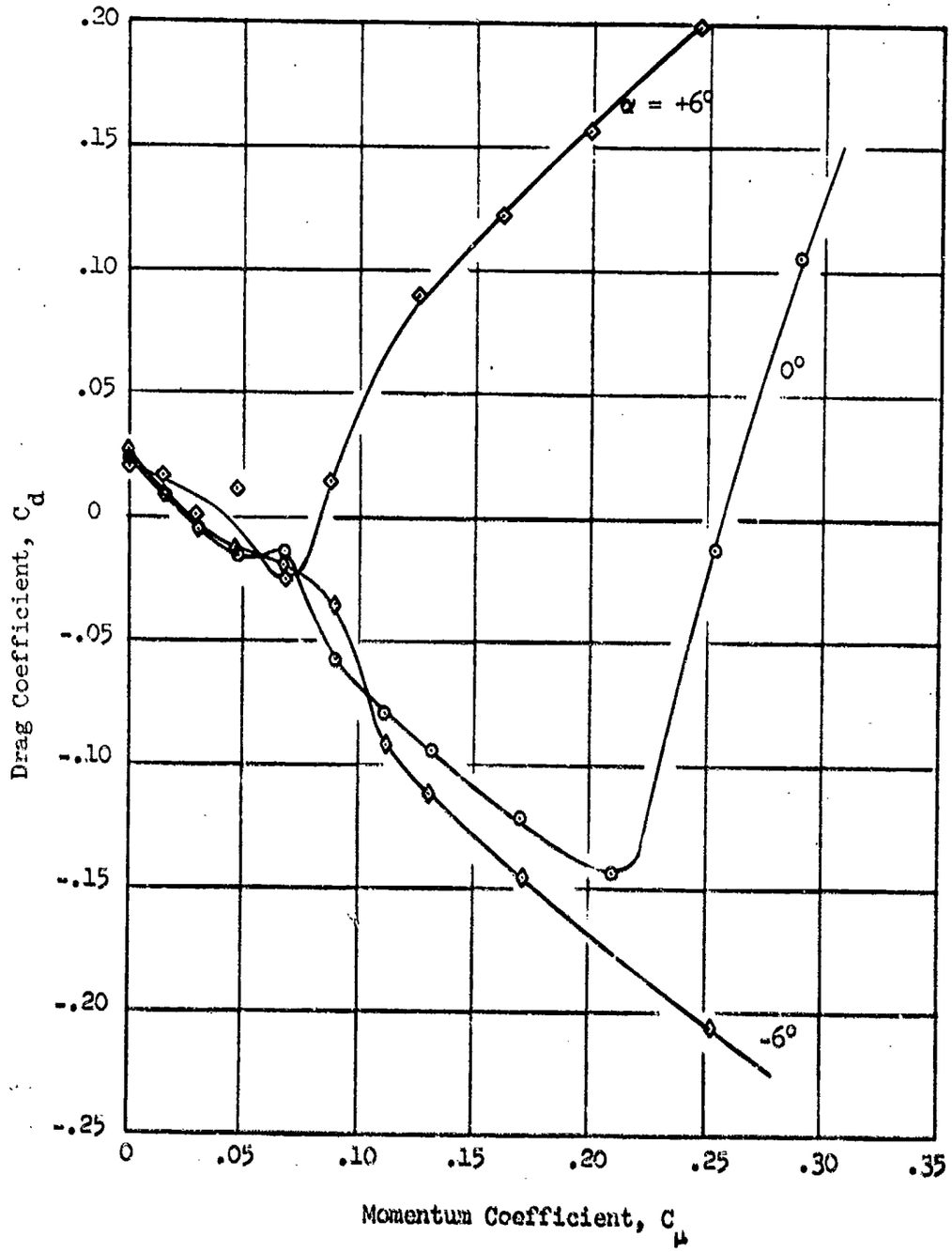

Figure 29 - Variation in Drag Coefficient for the Rounded Ellipse, h = 0.05 inch

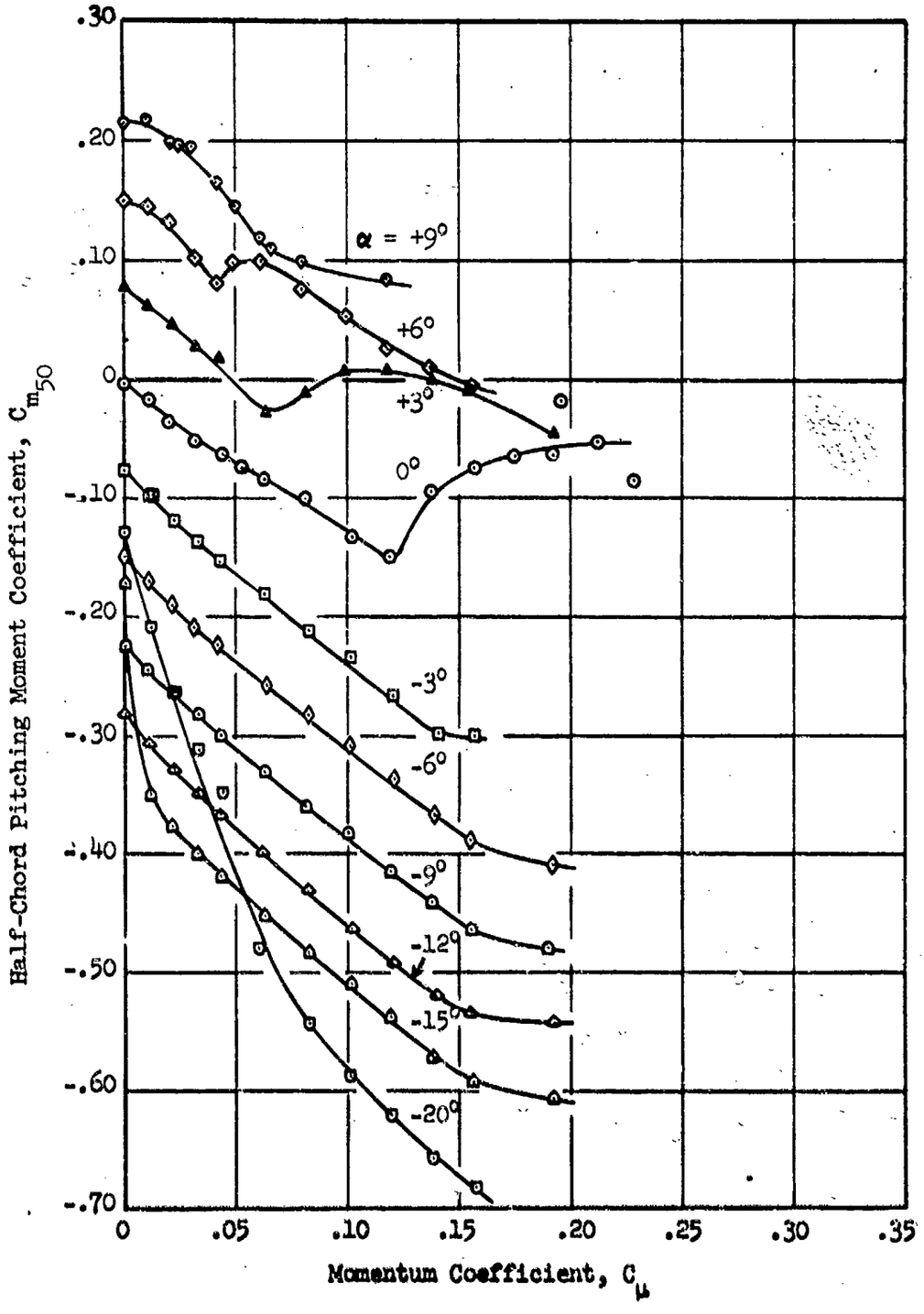

Figure 30 - Half-Chord Pitching Moment Coefficient for the Rounded Ellipse, h = 0.01 inch

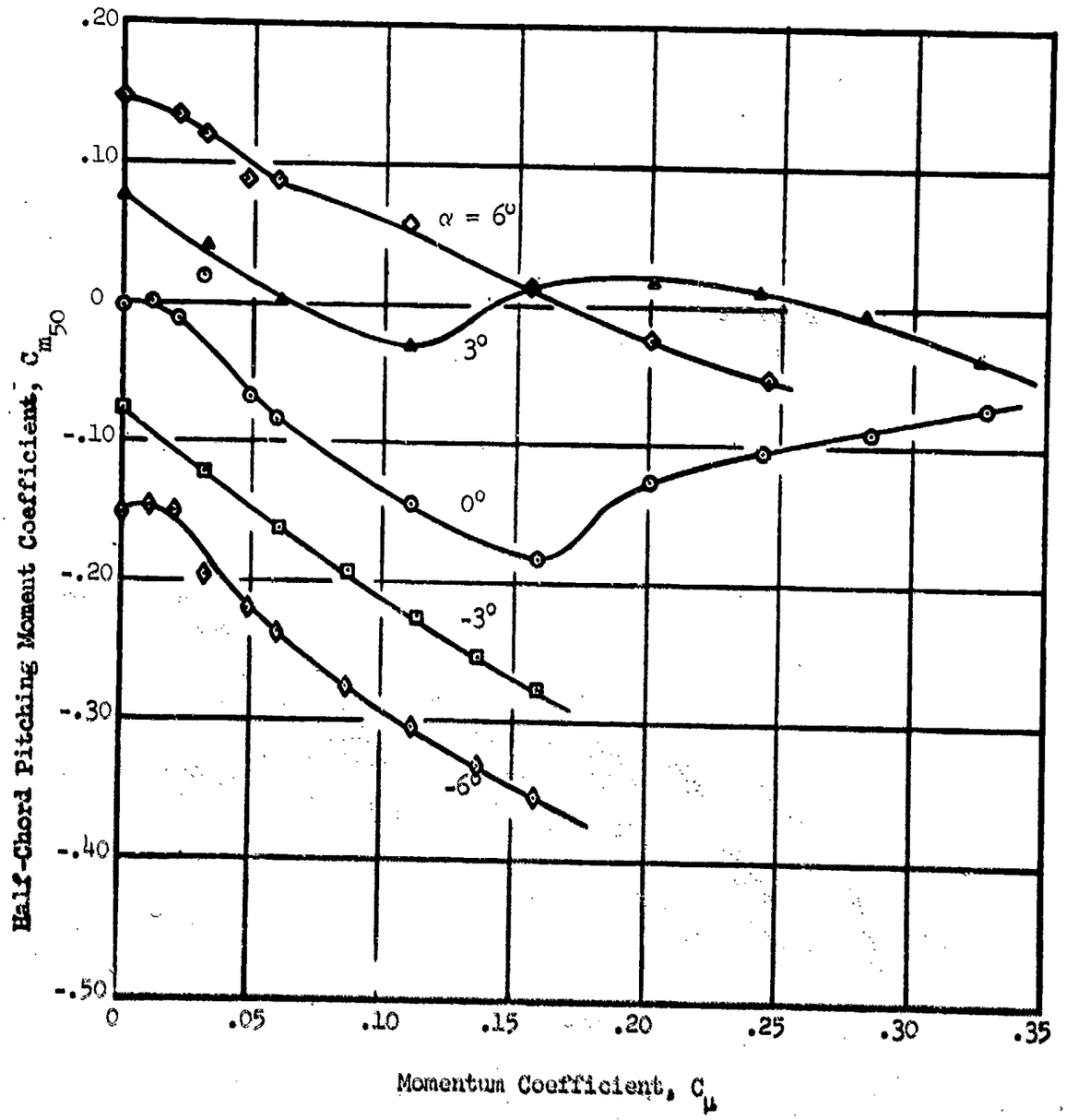

Figure 31 - Half-Chord, Pitching Moment Coefficient for the Rounded Ellipse, h = 0.025 inch

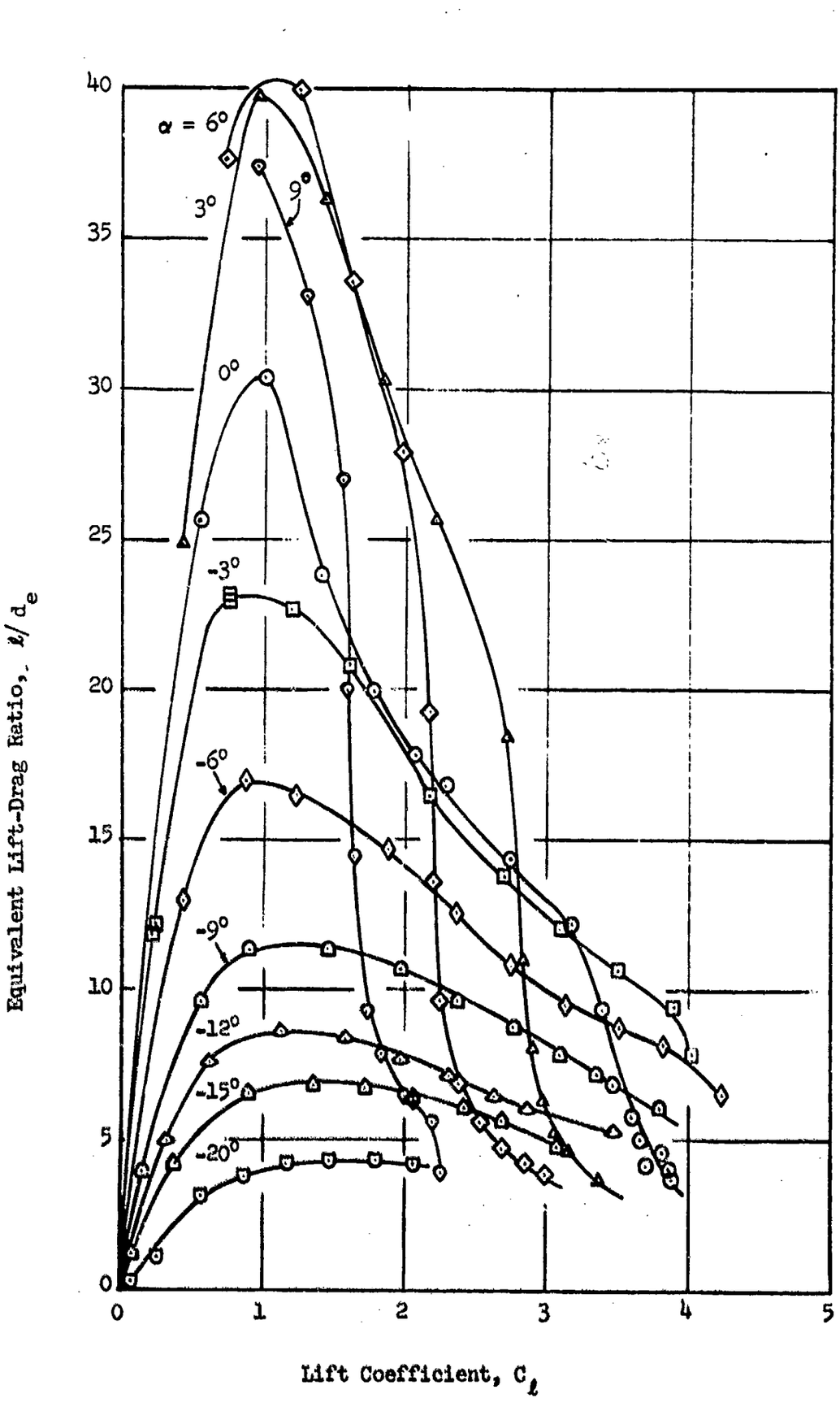

Figure 32 - Equivalent Lift-Drag Ratios for the Rounded Ellipse, h = 0.01 inch

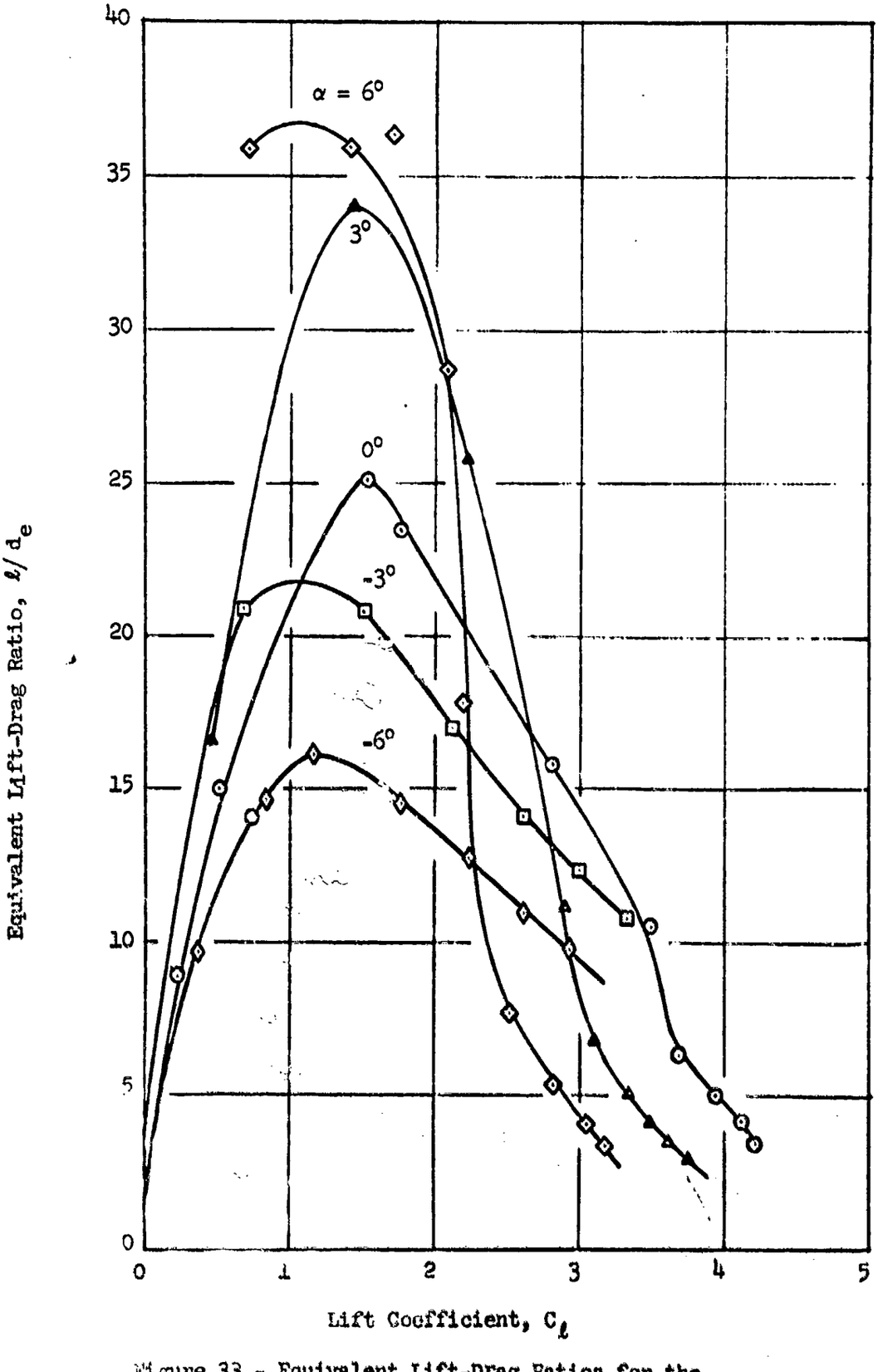

Figure 33 - Equivalent Lift-Drag Ratios for the Rounded Ellipse, h = 0.025 inch

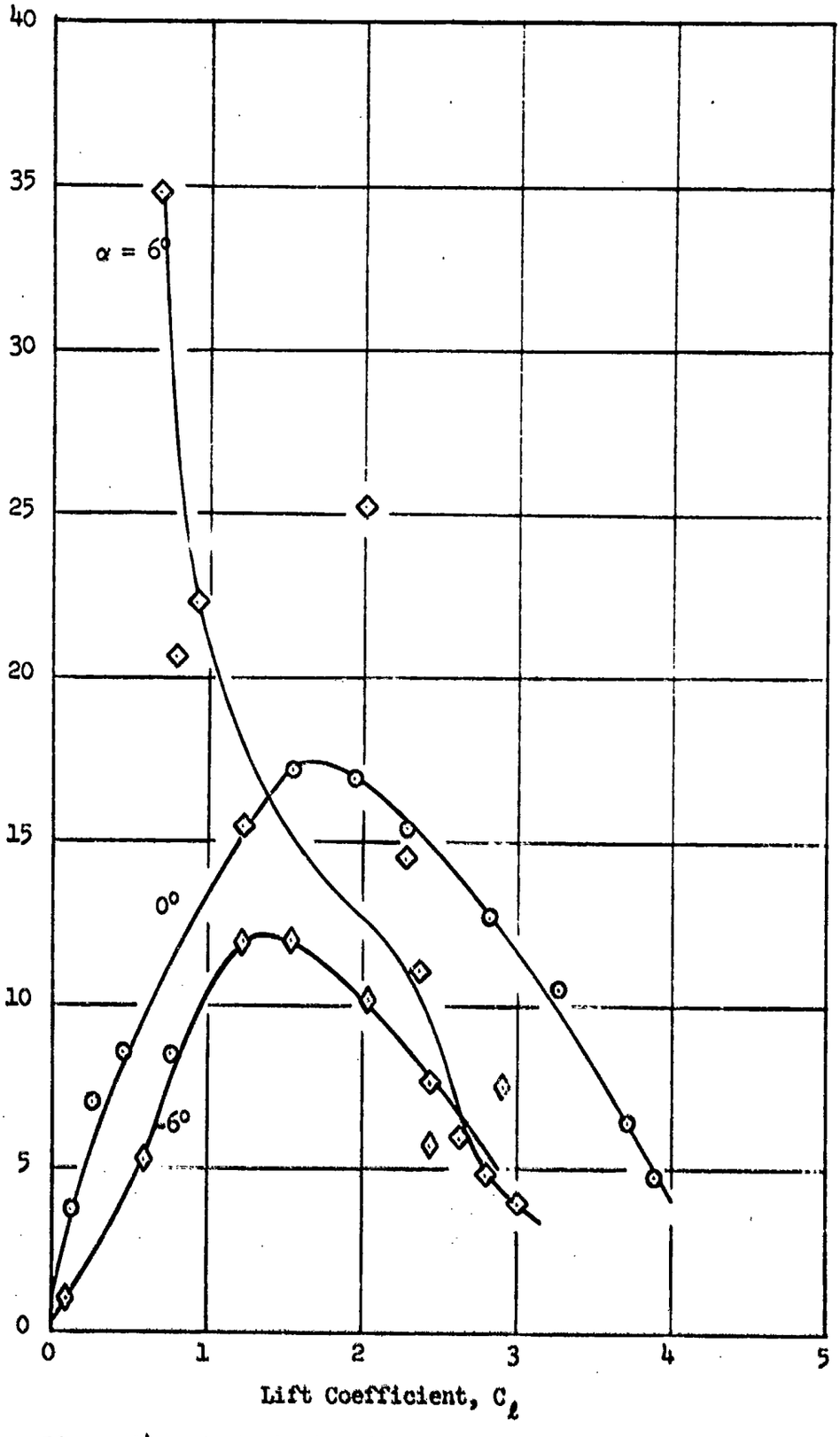

Figure 34 - Equivalent Lift-Drag Ratios for the Rounded Ellipse, h = 0.05 inch

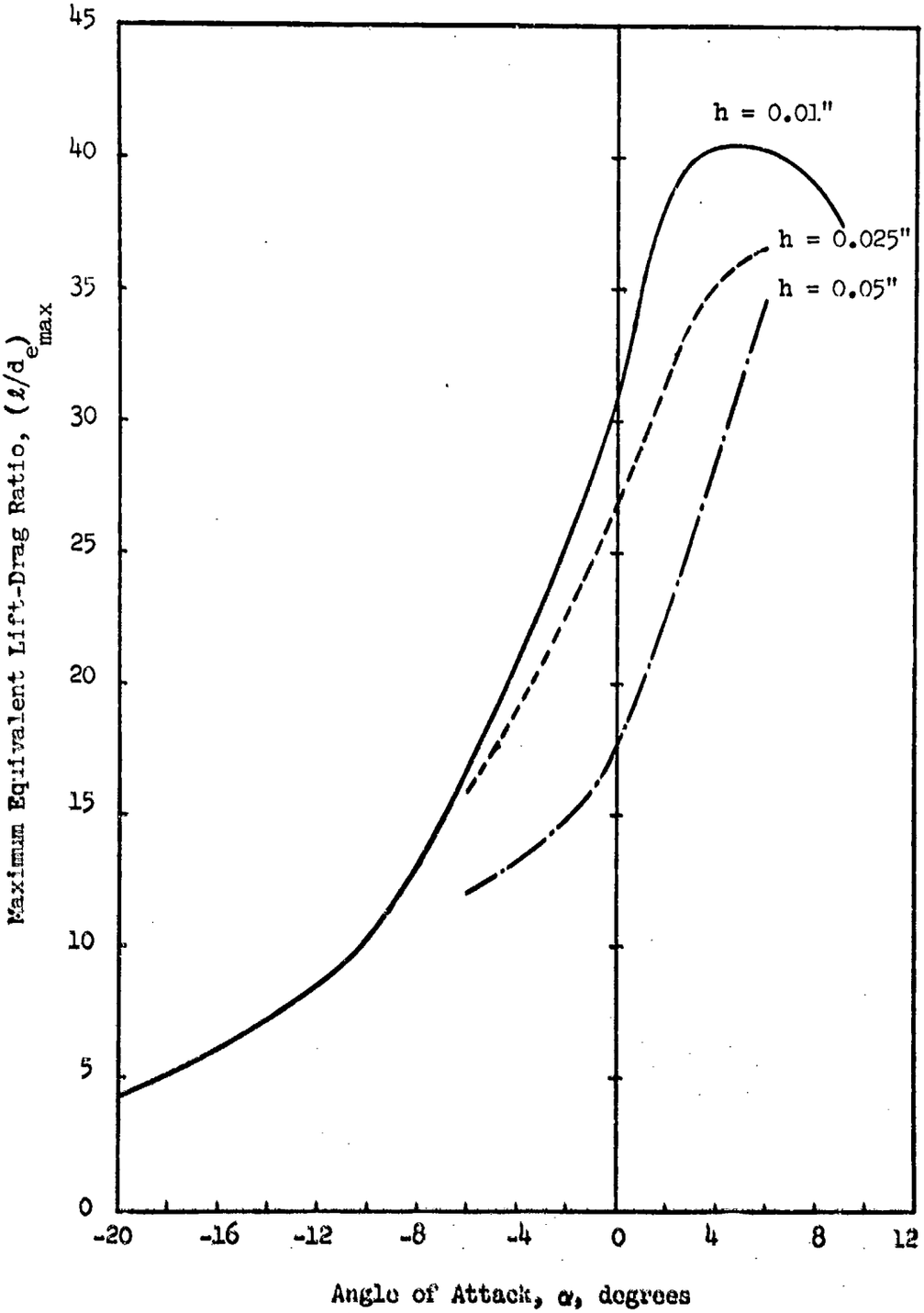

Figure 35 - Maximum Equivalent Lift-Drag Ratios for the Rounded Ellipse

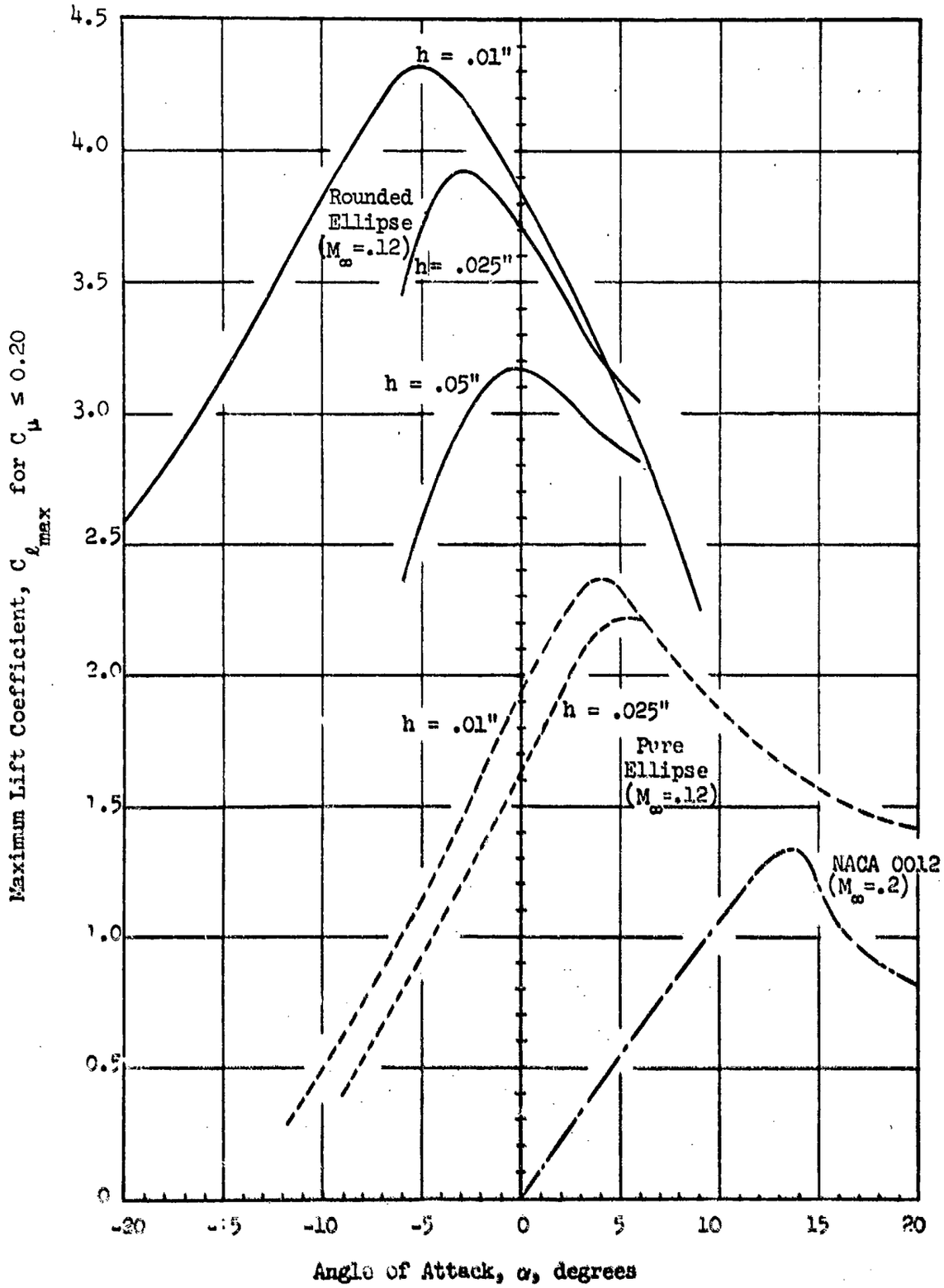

Figure 36 - Comparative Maximum Lift Coefficients of Circulation Control Sections With $C_\mu \leq 0.20$ and NACA 0012 Section

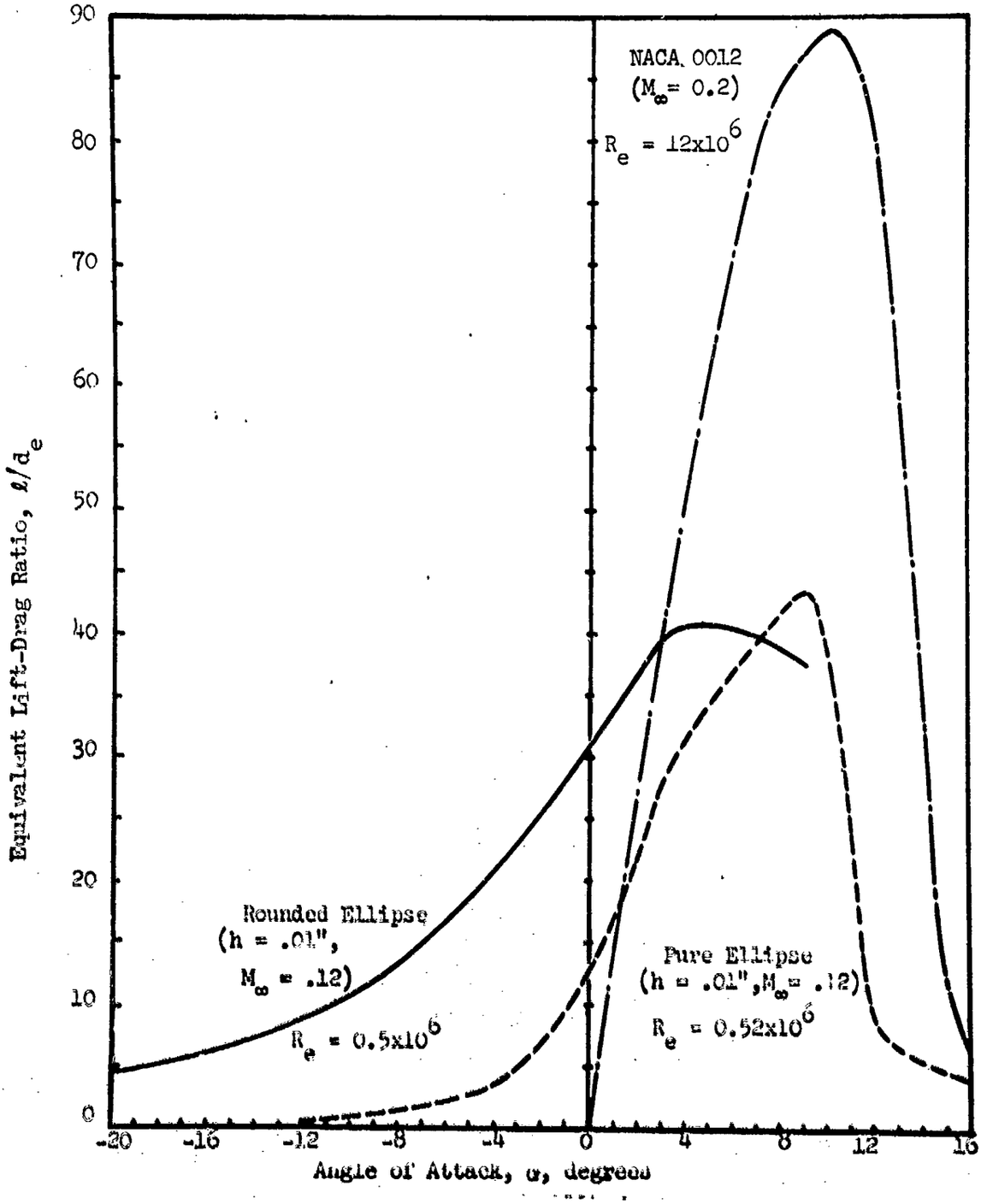

Figure 37 - Comparative Section Efficiencies for the Circulation Control Sections and NACA 0012

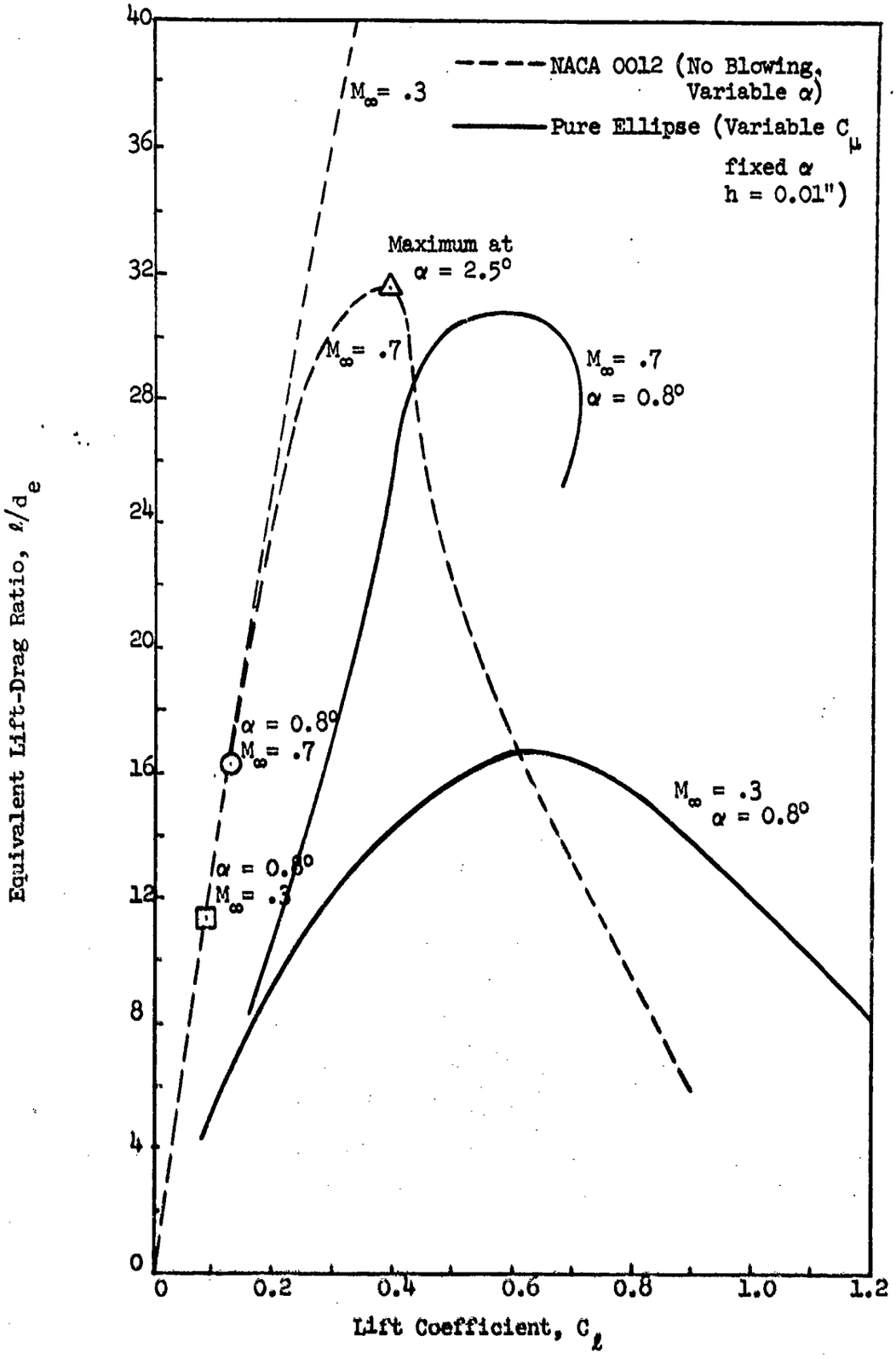

Figure 38 - Comparative Section Efficiencies for Subsonic and Transonic Mach Numbers

Distribution
not Shot

UNCLASSIFIED

Security Classification

DOCUMENT CONTROL DATA - R & D

(Security classification of title, body of abstract and indexing annotation must be entered when the overall report is classified)

1. ORIGINATING ACTIVITY *(Corporate author)*

Aviation and Surface Effects Department
Naval Ship Research and Development Center
Bethesda, Maryland 20034

2a. REPORT SECURITY CLASSIFICATION

UNCLASSIFIED

2b. GROUP

3. REPORT TITLE

TWO-DIMENSIONAL SUBSONIC WIND TUNNEL TESTS OF TWO 15-PERCENT THICK CIRCULATION CONTROL AIRFOILS.

4. DESCRIPTIVE NOTES *(Type of report and inclusive dates)*

Technical Note

5. AUTHOR(S) *(First name, middle initial, last name)*

Robert J. Englar

6. REPORT DATE	7a. TOTAL NO. OF PAGES	7b. NO. OF REFS
August 1971	63	11

8a. CONTRACT OR GRANT NO.	9a. ORIGINATOR'S REPORT NUMBER(S)
P0-1-0140	
b. PROJECT NO.	Technical Note AL-211
c.	9b. OTHER REPORT NO(S) *(Any other numbers that may be assigned this report)*
d. NSRDC 690-110	

10. DISTRIBUTION STATEMENT

Distribution limited to U.S. Government agencies only; Test and Evaluation; August 1971. Other requests for this document must be referred to Head, Aviation and Surface Effects Department.

11. SUPPLEMENTARY NOTES	12. SPONSORING MILITARY ACTIVITY (461)
	Office of Naval Research, Aeronautics Arlington, Virginia 22217

13. ABSTRACT

Two relatively thin Circulation Control (CC) elliptic airfoils were tested subsonically to determine their characteristics as proposed helicopter rotor tip sections. These airfoils, employing tangential trailing edge (Coanda) blowing, had shown very promising transonic characteristics in previous tests. It was the purpose of the subsonic retests to determine if these thin sections could generate low speed characteristics which would be equally impressive. Due to its more forward slot location, the 15-percent thick pure elliptic section displayed effective subsonic operation at positive angle of attack, reducing drag while producing lift coefficients up to 3.5. The rounded trailing edge configuration, with further aft slot and better Coanda deflection of the jet, generated lift coefficients up to 4.25 (with a preference for negative incidence), but experienced higher drag levels. As a result of the small nose radii and low test Reynolds number, both sections were limited in performance by leading edge separation. At a fixed momentum coefficient, variation in slot height indicated that better performance was obtained for reduced heights. This was due primarily to higher energy levels in the jet sheet, but the lower bound on slot height was limited by boundary layer building in very small nozzles. Comparison of both CC sections to the more conventional NACA 0012 blade section indicated far greater lift capabilities with circulation control. However, due to blowing power requirements, equivalent efficiency was less at positive incidence, than for the conventional section.

DD FORM 1 NOV 65 1473 (PAGE 1)

S/N 0101-807-6801

UNCLASSIFIED

Security Classification

Security Classification

14 KEY WORDS	LINK A		LINK B		LINK C	
	ROLE	WT	ROLE	WT	ROLE	WT

DD FORM 1 NOV 1473 (BACK)
(PAGE 2)

Security Classification